Acta Pharmaceutica Sinica B 2021;11(9):2859–2879

Chinese Pharmaceutical Association
Institute of Materia Medica, Chinese Academy of Medical Sciences

Acta Pharmaceutica Sinica B

www.elsevier.com/locate/apsb
www.sciencedirect.com

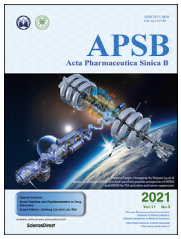

ORIGINAL ARTICLE

Novel compound FLZ alleviates rotenone-induced PD mouse model by suppressing TLR4/MyD88/NF-κB pathway through microbiota–gut–brain axis

Zhe Zhao, Fangyuan Li, Jingwen Ning, Ran Peng, Junmei Shang, Hui Liu, Meiyu Shang, Xiu-Qi Bao, Dan Zhang*

State Key Laboratory of Bioactive Substrate and Function of Natural Medicine, Institute of Materia Medica, Chinese Academy of Medical Sciences and Peking Union Medical College, Beijing 100050, China

Received 2 November 2020; received in revised form 7 January 2021; accepted 12 February 2021

KEY WORDS

FLZ;
Microbiota–gut–brain axis;
Parkinson's disease;
Rotenone mouse model;
TLR4/MyD88/NF-κB pathway;
Gastrointestinal dysfunction;
Systemic inflammation;
Neuroinflammation

Abstract Parkinson's disease (PD) is the second most common neurodegenerative disease, but none of the current treatments for PD can halt the progress of the disease due to the limited understanding of the pathogenesis. In PD development, the communication between the brain and the gastrointestinal system influenced by gut microbiota is known as microbiota–gut–brain axis. However, the explicit mechanisms of microbiota dysbiosis in PD development have not been well elucidated yet. FLZ, a novel squamosamide derivative, has been proved to be effective in many PD models and is undergoing the phase I clinical trial to treat PD in China. Moreover, our previous pharmacokinetic study revealed that gut microbiota could regulate the absorption of FLZ *in vivo*. The aims of our study were to assess the protective effects of FLZ treatment on PD and to further explore the underlying microbiota-related mechanisms of PD by using FLZ as a tool. In the current study, chronic oral administration of rotenone was utilized to induce a mouse model to mimic the pathological process of PD. Here we revealed that FLZ treatment alleviated gastrointestinal dysfunctions, motor symptoms, and dopaminergic neuron death in rotenone-challenged

Abbreviations: ANOSIM, adonis and analysis of similarity; α-Syn, α-synuclein; BBB, blood–brain barrier; CFU, colony-forming units; CMC-Na, sodium carboxymethyl cellulose; CNS, central nerve system; ELISA, enzyme-linked immunosorbent assay; FD4, FITC-dextran (MW: 4 kDa); FITC, fluorescein isothiocyanate; GFAP, glial fibrillary acidic protein; GI, gastrointestinal; Hp, *Helicobacter pylori*; Iba-1, ionized calcium-binding adapter molecule 1; IL-1β, interleukin-1β; IL-6, interleukin-6; KEGG, Kyoto Encyclopedia of Genes and Genomes; LBP, lipopolysaccharide binding protein; LDA, linear discriminant analysis; LPS, lipopolysaccharide; MLNs, mesenteric lymph nodes; OTU, operational taxonomic unit; PBS, phosphate-buffered saline; PCoA, principal coordinate analysis; PD, Parkinson's disease; qPCR, quantitative polymerase chain reaction assay; SD, standard deviation; SN, substantia nigra; TEM, transmission electron microscopy; TH, tyrosine hydroxylase; TLR4, toll-like receptor 4; TNF-α, tumor necrosis factor-α.

*Corresponding author.
E-mail address: danzhang@imm.ac.cn (Dan Zhang).

Peer review under responsibility of Chinese Pharmaceutical Association and Institute of Materia Medica, Chinese Academy of Medical Sciences.

https://doi.org/10.1016/j.apsb.2021.03.020

mice. 16S rRNA sequencing found that PD-related microbiota alterations induced by rotenone were reversed by FLZ treatment. Remarkably, FLZ administration attenuated intestinal inflammation and gut barrier destruction, which subsequently inhibited systemic inflammation. Eventually, FLZ treatment restored blood−brain barrier structure and suppressed neuroinflammation by inhibiting the activation of astrocytes and microglia in the substantia nigra (SN). Further mechanistic research demonstrated that FLZ treatment suppressed the TLR4/MyD88/NF-κB pathway both in the SN and colon. Collectively, FLZ treatment ameliorates microbiota dysbiosis to protect the PD model *via* inhibiting TLR4 pathway, which contributes to one of the underlying mechanisms beneath its neuroprotective effects. Our research also supports the importance of microbiota−gut−brain axis in PD pathogenesis, suggesting its potential role as a novel therapeutic target for PD treatment.

1. Introduction

Parkinson's disease (PD) is well known as the second most common neurodegenerative disease with an estimated prevalence of 0.1%−0.2% worldwide, involving both motor dysfunctions as well as non-motor symptoms[1]. Main motor dysfunctions, including tremor, bradykinesia, and rigidity, are acknowledged to be caused by the deficit of dopaminergic neurons in the substantia nigra (SN) pars compacta, which is a key feature of PD[2]. As another critical pathological feature of PD, Lewy bodies characterized by intracellular aggregates of misfolded α-synuclein (α-Syn) are found not only in the central nerve system (CNS, brain and spinal cord), but also in the sympathetic ganglia, enteric nervous system, vagus nerve, sciatic nerve and the cutaneous nerves[3−5].

Moreover, a wide range of non-motor symptoms involving common gastrointestinal (GI) dysfunctions, like dysphagia, nausea, vomiting, and constipation are reported to show greater negative effects on the life quality of PD patients compared to motor symptoms[6,7]. It is reported that these GI dysfunctions happen many years prior to motor symptoms, which supports the hypothesis that PD may derive from gut[8]. Further evidence proves that the close communication between the brain and the GI system is affected by gut microbiota in the pathogenesis of PD, known as microbiota−gut−brain axis[4,9]. The high rate of *Helicobacter pylori* (Hp) infection was found in PD patients many years ago[10]. Recent microbial analysis of feces revealed that the bacterial family Verrucomicrobiaceae (*Akkermansia* genus) abundance and unclassified Firmicutes phylum increased, while the genera *Prevotella copri* and *Eubacterium biforme* were reported to remarkedly decrease in PD patient feces[11]. Another study found that the abundance of Prevotellaceae family reduced in PD patients compared to healthy individuals, whereas higher levels of Enterobacteriaceae were detected in PD patients with severer postural difficulty and gait instability[12]. All these data prove that microbiota dysbiosis plays a critical role in the PD pathogenesis.

Although evidence of gut microbiota alterations in PD patients has been increasingly reported, the explicit mechanisms beneath the microbiota dysbiosis are still far from well elucidated. Many researches have proved that pathological alterations of microbiota composition not only induce chronic intestinal inflammation and increased gut permeability, but also lead to neuroinflammation[13−15]. Activated by the conserved endotoxin molecules derived from altered microbiota, like lipopolysaccharide (LPS) in the gut, toll-like receptor 4 (TLR4) and its downstream pathway would locally elevate the inflammation and permeability of the gut[16−18]. As a consequence of gut leakiness, microbial LPS released into tissues further stimulates the TLR4 pathway in the immune cells to secrete pro-inflammatory cytokines in the gut as well as the systemic circulation, including Interleukin-1β (IL-1β), Interleukin-6 (IL-6) and tumor necrosis factor-α (TNF-α)[19−21]. Then, these increased levels of inflammatory cytokines and endotoxin LPS cross the blood−brain barrier (BBB) to prompt subsequent neuroinflammation[20,22,23]. However, more investigations are still needed to explain the mechanisms of microbiota−gut−brain axis in PD development.

Since the specific mechanisms of PD development are not clear, current therapies for PD can only exert symptomatic effects rather than stop the progress of the neurodegeneration. Therefore, the discovery of novel drugs is in urgent need to develop effective therapeutic strategies for PD. FLZ, a novel synthetic derivative of squamosamide, illustrated significant effects on protecting several *in vivo* and *in vitro* PD models in our previous reports and is now undergoing phase I clinical study to treat PD in China[24]. However, the specific mechanisms of its neuroprotective effects on PD have not been fully elucidated. Our previous pharmacokinetic study revealed that gut microbiota mediates the absorption of FLZ and further regulates its therapeutic effects on PD. Several studies have demonstrated that the chronic oral administration of rotenone could well reproduce the spatiotemporal process of pathological presentations and clinical manifestations of PD patients[25−28]. Moreover, a recent longitudinal study illustrated that orally administrated rotenone induced microbiota dysbiosis and gastrointestinal dysfunctions prior to CNS pathology and motor symptoms, suggesting that the development of this model is closely associated with gut microbiome[18]. Therefore, chronic rotenone model is an appropriate model to evaluate effects of drug candidates for PD treatment and to investigate the mechanisms of microbiota dysbiosis in PD. In the current research, rotenone-induced mouse model was established to assess the protective effects of FLZ on PD symptoms and to explore its potential mechanisms of microbiota−gut−brain axis in protecting PD models.

Taken together, we hypothesized that the microbial dysbiosis induced by rotenone could lead to the inflammation and barrier destruction in the gut and brain *via* TLR4 pathways in PD pathogenesis and FLZ treatment could reverse the development. Our objectives were to evaluate the protective effects of FLZ administration on PD and to further explore its underlying microbiota-related mechanisms. Moreover, we also aimed to discover the explicit mechanisms of microbiota−gut−brain axis in PD by using FLZ as a tool.

2. Materials and methods

2.1. Agents

FLZ, a novel synthetic derivative of squamosamide from a Chinese herb with 99% purity, was provided by the Department of Pharmaceutical Chemistry, Institute of Materia Medica, Chinese Academy of Medical Sciences and Peking Union Medical College, Beijing, China. The compound FLZ, formulated as *N*-[2-(4-hydroxy-phenyl)-ethyl]-2-(2,5-dimethoxy-phenyl)-3-(3-methoxy-4-hydroxy-phenyl)-acrylamide (Fig. 1A), was suspended in 0.5% sodium carboxymethyl cellulose (CMC-Na, Sigma−Aldrich, St. Louis, MO, USA) for administration. Rotenone (Sigma−Aldrich) was suspended in 4% carboxymethylcellulose (Sigma−Aldrich) and 1.25% chloroform (Beijing Chemical Works, Beijing, China).

2.2. Animals

Male C57BL/6J mice (aging 8 weeks old; weighing 20−22 g) were supplied by Beijing Vital River Laboratory Animal Technology Co., Ltd. (Beijing, China). All the animals were acclimatized for seven days under standard conditions (temperature 22 ± 2 °C and humidity 50%−60% on a 12 h light/dark cycle) with free access to water and standard chow. All the experimental procedures were performed in accordance with the guidelines of the Beijing Municipal Ethics Committee for the care and use of laboratory animals, and were approved by the Animal Care & Welfare Committee, Institute of Materia Medica, CAMS & PUMC (No. 00005402).

2.3. Rotenone model induction and treatments

Before Week 4, a total of 65 male C57BL/6 J mice were randomly divided into Control group (n = 25) and Model group (n = 40). Briefly, the Model group mice were orally administrated with freshly prepared rotenone solution (30 mg/kg body weight) once a day for four weeks[18,29]. Simultaneously, the Control group mice received an oral administration of vehicle. Five mice from each group were sacrificed at Weeks 3 and 4, respectively (Fig. 1B). Thereafter, the remaining 30 mice in Model group were randomly classified into two groups: Rotenone group (n = 15) and FLZ group (n = 15). While, the 15 remaining mice in Control group were still named Control group. From Week 4, the mice in the FLZ group were orally fed with FLZ (75 mg/kg/day) for two weeks, and the dose of FLZ was optimized based on our previous studies[24,30]. The Control and Rotenone group mice were treated with vehicle during this period. All the mice were weighted every day during these six weeks. In the meantime, GI function tests and fecal collection were performed weekly and behavioral tests were administrated at Weeks 3, 4 and 6, respectively. The whole procedure of mice treatment is shown in Fig. 1B.

2.4. Fecal pellets output

A total of 45 mice were forced to fast for 2 h, and then each mouse was arranged in a clean, clear plastic cages for 2 h. Fecal pellets were collected and placed in sealed tubes. Subsequently, the numbers of fecal pellets were counted. Then, the feces were weighed to get the wet weight and dried at 85 °C for 24 h to obtain the dry weight. The water content was calculated according to the difference between the wet and dry fecal pellets weight.

In addition, measurements of gut motor function were evaluated by 20 min stool collection. Each of the 45 mice was assigned in a clean and clear plastic cage. The number of fecal pellets were recorded at 5 min intervals for a 20 min period.

2.5. Intestinal transit and colon length

Mice were orally administrated with 0.3 mL 2.5% Evans blue (Sigma−Aldrich) suspended in 1.5% CMC-Na (Sigma−Aldrich) 30 min before sacrifice. Then the distance between the pylorus and the most distal point was measured as the intestinal transit distance[31]. Additionally, the length of colon (from the end of cecum to the anus) was recorded.

2.6. Behavioral tests

Four behavioral tests were performed to evaluate the motor functions. All the mice underwent the four tests with an interval of 1 h between each test.

2.6.1. Rotarod test

Mice were placed on the rotarod and then tested at a speed of 30 rpm for up to 120 s on the revolving rod. The time when the mice first fell off the rod was automatically recorded by the rotarod, which was designated as latency. Each mouse was tested three times. Between each trial, mice were allowed to rest for 1 h.

2.6.2. Pole test

The pole includes a 50 cm wooden pole (3 cm in diameter) and a wooden ball. The base of pole was positioned in the home cage and the wooden ball was fixed on top of the pole to prevent mice from sitting on the top and to help position the mice on the pole. The performance of mice descending the pole was scored by a scale of 0−5. The mice were pretrained before experimentation. Each mouse performed three trials with an interval of 1 h.

2.6.3. Adhesive removal test

Mice were placed into a clean cage and allowed to move freely for 3 min before the test for acclimation. Round adhesive stickers were attached to the front paws of the mice with slight pressure. Then they were placed back into the cage and time for each mouse to completely remove the stickers was recorded. Three trials were administrated for each animal and they were allowed an interval of 30 min between each trial.

2.6.4. Hanging grip test

The front paws of the mice were made to grasp the horizontal rope (about 5 mm in diameter). Then they were observed and assigned a score from 0 to 5, which was based on the following criteria: 0, dropping from the rope within 10 s; 1, gripping the rope with one front paw; 2, gripping the rope with both front paws; 3, gripping the rope with one hind paw; 4, gripping the rope with both hind paws; 5, attempting to escape to the end of the horizontal rope. The test was performed three times for each mouse with an interval of 1 h.

2.7. Bacterial translocation study

Samples of livers, spleens, and mesenteric lymph nodes (MLNs) were removed under sterile conditions at sacrifice and performed as described below. The samples were weighed and homogenized in 0.9% sterile saline at a ratio of 1:9 (0.1 g tissue sample, 0.9 mL

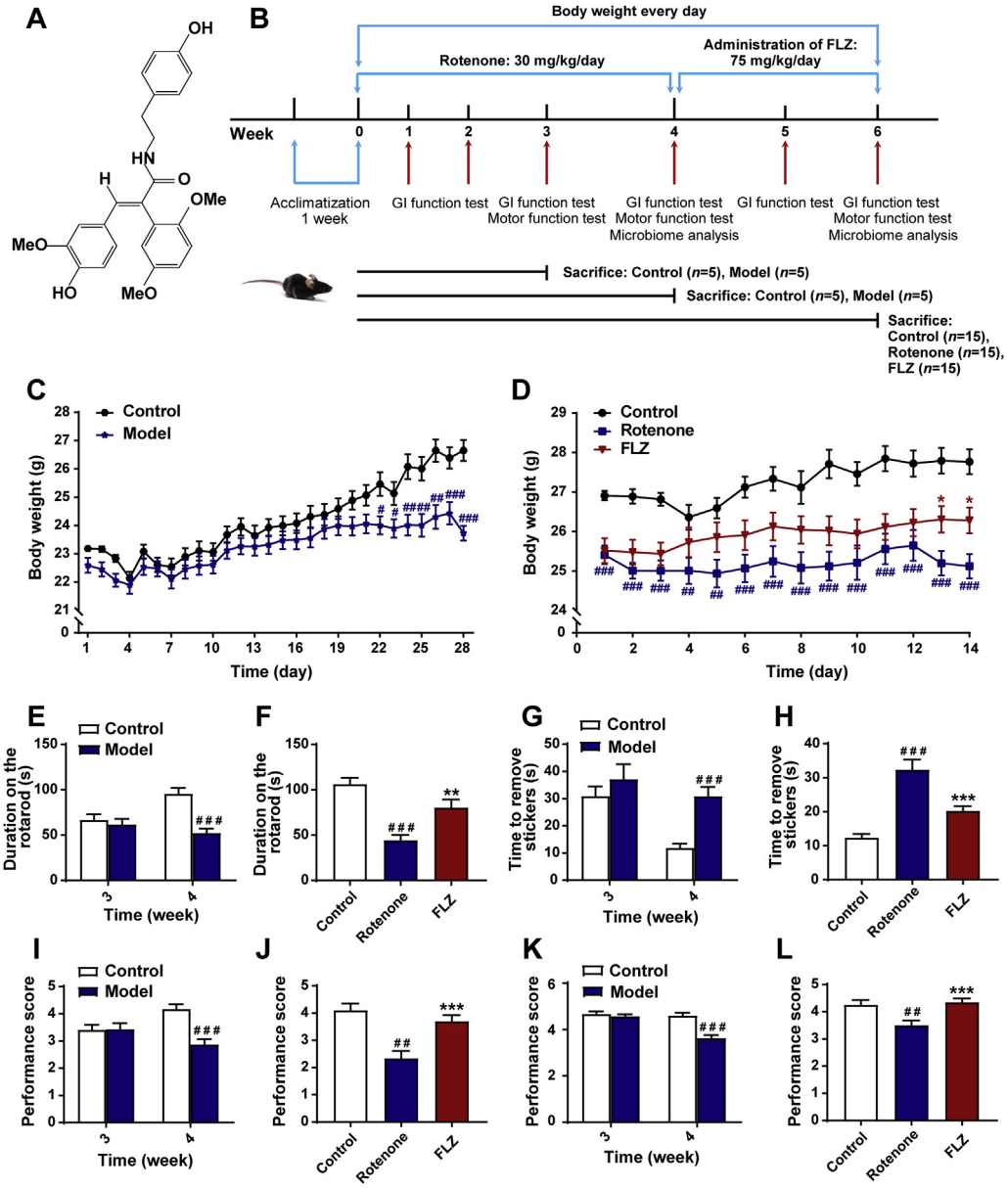

Figure 1 FLZ treatment alleviates weight loss and motor dysfunctions of the rotenone-induced PD mice. (A) The chemical structure of FLZ. (B) The flow chart of animal treatments. (C) The body weight of mice from Weeks 1−4 (n = 15 for Control group; n = 30 for Model group). (D) The body weight of mice from Weeks 5−6 (n = 15 for each group). (E)−(F) Rotarod tests in Weeks 3−4 (E) and Week 6 (F). (G)−(H) Adhesive removal tests in Weeks 3−4 (G) and Week 6 (H). (I)−(J) Hanging grip test in Weeks 3−4 (I) and Week 6 (J). (K)−(L) Pole test scores in Weeks 3−4 (K) and Week 6 (L). For behavioral tests in Weeks 3−4, n = 15 for the Control group; n = 30 for the Model group. For behavioral tests in Weeks 5−6, n = 15 for each group. Data are presented as mean ± SD. $^{\#}P < 0.05$, $^{\#\#}P < 0.01$, $^{\#\#\#}P < 0.001$ *versus* the Control group; $^{*}P < 0.05$, $^{**}P < 0.01$, $^{***}P < 0.001$ *versus* the Rotenone group.

0.9% sterile saline). Then 100 μL of 10-fold dilutions of the suspension were plated onto Lysogeny Broth agar plates. The numbers of colony-forming units (CFUs) were calculated and analyzed after incubating at 37 °C for 24 h.

2.8. *In vivo intestinal permeability assay of FITC-dextran*

In vivo intestinal permeability assessment was carried out using fluorescein isothiocyanate-dextran (FITC-dextran, FD4; MW: 4 kDa, Sigma−Aldrich). Briefly, mice were forced to fast for 4 h and then received an oral administration of FD4 (0.6 mg/g body weight). Four hours later, the mice were euthanized and serum was obtained after retro-orbital puncture. Serum fluorescence intensity was subsequently assessed at 485/525 nm by a fluorescence spectrophotometer. FD4 concentrations were determined using a standard curve generated by serial dilution of FD4 in phosphate-buffered saline (PBS).

2.9. *Immunofluorescence staining*

Five mice were randomly selected from each group and deeply anesthetized, then they were perfused transcardially with saline infusion followed by 4% paraformaldehyde in 0.1 mol/L PBS. The brains and colons were removed and fixed in 4%

paraformaldehyde for 24 h. Then the tissues were kept in 4% paraformaldehyde containing 30% sucrose. Brains were embedded in paraffin and sectioned into 5 μm through the SN. Colons were embedded in paraffin and serially sliced at a 5-μm thickness. The immunofluorescence staining was performed following our previous research[32]. Briefly, the sections were deparaffinized and rehydrated. Next, they were immersed in sodium citrate solution (pH 6.0) for antigen retrieval. Subsequently, 3% bovine serum albumin (Servicebio, Wuhan, China) was added to block nonspecific binding and the slides were incubated overnight at 4 °C with the following primary antibodies: anti-TLR4 (1:50, Santa Cruz Biotechnology, CA, USA), anti-ZO-1 (1:100, Thermo Fisher Scientific, Waltham, MA, USA), anti-tyrosine hydroxylase (TH, 1:1000, Servicebio), anti-glial fibrillary acidic protein (GFAP, 1:1000, Servicebio), and anti-ionized calcium-binding adapter molecule 1 (Iba-1, 1:1000, Servicebio). Then the objective tissues were covered with corresponding secondary antibodies: FITC labeled goat anti-mouse (1:400, Servicebio); goat anti-mouse IgG-CY3 (1:300, Servicebio) and goat anti-rabbit IgG-CY3 (1:300, Servicebio). Nuclei were stained using DAPI solution. The images were observed with fluorescent microscopy (Nikon Eclipse C1, Tokyo, Japan) and the number of positively stained cells was calculated using Image Pro Plus 6.0 software. All evaluations were done by a researcher blind to the experiment. Each section was quantified based on 5 randomly selected fields.

2.10. *Transmission electron microscopy*

The anesthetized mice were perfused with 0.9% saline, and 1 mm^3 SN and colon tissue blocks were taken. Next, the fresh tissue blocks were put into Fixative for transmission electron microscopy (TEM, Servicebio) at 4 °C for 4 h and then fixed with 1% OsO4 in 0.1 mol/L PBS for 2 h at room temperature, followed by dehydration with gradient alcohol. Subsequently, the sections were embedded by baking in an oven at 60 °C for 48 h and cut into ultrathin sections (60 nm) with ultramicrotome. Finally, the ultrastructure of tight junction of the brain and colon were observed using a transmission electron microscope (HITACHI, HT7700, Japan).

2.11. *Quantitative polymerase chain reaction assay*

The total RNA was isolated from the SN or colon tissues using the TransZol Up Plus RNA kit (TransGen Biotech Co., Beijing, China) according to the manufacturer's instructions. Then the amount of RNA was reversely transcribed to cDNA using TransScript One-Step gDNA Removal and cDNA Syn-thesis SuperMix (TransGen Biotech Co.). Quantitative polymerase chain reaction assay (qPCR) of different genes was detected by TransStart Tip Green qPCR SuperMix (+DyeI/+DyeII) (TransGen Biotech Co.), and the mRNA was amplified for qPCR with the following primers shown in Table 1. Amplification was run in the 7900HT Fast Real-Time PCR system (Applied Biosystems, Foster City, CA, USA) at 94 °C for 30 s followed by 40 cycles of 94 °C for 5 s, 59 °C for 15 s, and 72 °C for 10 s, then 95 °C for 15 s as a final elongation step. The relative quantification of mRNA expression was calculated by $2^{-\Delta\Delta Ct}$ algorithms.

2.12. *Enzyme-linked immunosorbent assay*

Mouse LPS endotoxin, lipopolysaccharide binding protein (LBP), IL-1β, IL-6, and TNF-α enzyme-linked immunosorbent assay (ELISA) kits were provided by Jianglai Industrial Limited By Share Ltd., Shanghai, China. All the experimental procedures were performed following the instructions recommended by the manufacturer. The cytokine concentrations were calculated by standard protein concentration.

2.13. *Fecal DNA extraction and microbiota sequencing*

We randomly chose 5 and 7 mice from each group respectively at Weeks 4 and 6 to collect feces for RNA sequencing. Every mouse was placed individually in an empty autoclaved cage and allowed to defecate freely after the last treatment. 6−8 fresh fecal pellets were collected from each mouse and were immediately placed into an individual sterile EP tube. All samples were then frozen instantly and stored at −80 °C prior to analyses. DNA was extracted from each fecal sample using improved protocol based on the guidelines of QIAamp Fast DNA Stool Mini Kit (Qiagen, Germany). The V3−V4 region of the bacteria 16S ribosomal RNA genes were amplified using barcoded primers: forward primer (5′−3′): CCTACGGGRSGCAGCAG (341 F) and reverse primer (5′−3′): GGACTACVVGGGTATCTAATC (806 R) with a denaturation step at 95 °C for 3 min, followed by 30 cycles at 98 °C for 20 s, 58 °C for 15 s, and 72 °C for 20 s and a final extension at 72 °C for 5 min. All quantified amplicons were pooled to equalize concentrations for sequencing using Illumina MiSeq (Illumina, Inc., CA, USA). DNA extraction, library construction and sequencing were conducted by Realbio Genomics Institute (Shanghai, China).

2.14. *Bioinformatic analysis*

Raw data processing and data analysis services were provided by Realbio Genomics Institute (Shanghai, China). Briefly, the paired end reads of 300 bp were overlapped on their 3′ ends for concatenation into original longer tags by using PANDAseq[33]. Then, Operational Taxonomic Units (OTUs) were clustered by Usearch (V7.0.1090)[34] for further annotation of taxonomic levels from phylum to genus based on Ribosomal Database Project (RDP, http://rdp.cme.msu.edu)[35,36]. Alpha-diversity indices were calculated based on relative abundances of known OTUs using QIIME (V1.9.1)[37]. Beta-diversity was analyzed by weighted Unifrac distances and then group differences were compared by adonis and analysis of similarity (ANOSIM) tests, displayed by principal coordinate analysis (PCoA). Linear discriminant analysis (LDA) was conducted to compare the differences of microbial community compositions among groups using LDA EffectSize Tools (V1.0)[38]. Finally, the functional prediction was analyzed using Phylogenetic Investigation of Communities by Reconstruction of Unobserved States (PICRUSt) to identify enrichment of Kyoto Encyclopedia of Genes and Genomes (KEGG) pathways[39]. The comparisons of alpha-diversity and microbial community differences among different groups were performed using Kruskal−Wallis test followed by the Mann−Whitney U test on R (V3.5.1). In addition, PCoA, heatmap and boxplots were analyzed by R (V3.5.1).

2.15. *Western blot*

For Western blot, the SN and colon tissues were separated and lysed in RIPA lysis buffer (C1055, APPLYGEN, China) including protease phosphatase inhibitor (P1260, APPLYGEN, China) and protease inhibitor (P1265, APPLYGEN, China). Then

Table 1 Primers used for quantitative PCR.

Gene	Primer sequence (5′−3′)	
	Forward	Reverse
Il6	CTGCAAGAGACTTCCATCCAG	AGTGGTATAGACAGGTCTGTTGG
Il1b	GCTACCTATGTCTTGCCCGT	GACCATTGCTGTTTCCTAGG
Iba1	ATCAACAAGCAATTCCTCGATGA	CAGCATTCGCTTCAAGGACATA
Cox 2	GAAGTGGGGGTTTAGGATCATC	CCTTTCACTTTCGGATAACCA
Cd3	ACGATGCCGAGAACATTGAA	TGGGTTGGGAACAGGTGGTG
Tnf	ACGGCATGGATCTCAAAGAC	AGATAGCAAATCGGCTGACG
Nos 2	CAGCTGGGCTGTACAAACCTT	CATTGGAAGTGAAGCGTTTCG
Zo1	TTCCCAGCTTATGAAAGGGTT	TCGCTTCTTTCAGGGCACCGTA
Cldn5	ACTGCCTTCCTGGACCACAAC	CGCCAGCACAGATTCATACACCT
Ocln	TTACAGGCAGAACTAGACGAC	TGATGTGCGATAATTTGCTCT
Gfap	AACAACCTGGCTGCGTAT	CTGCCTCGTATTGAGTGC
Cldn1	GCCATCTACGAGGGACTG	GAGCAGGAAAGTAGGACACC
Tlr4	AACTTCAGTGGCTGGATT	ACTAGGTTCGTCAGATTGG
Gapdh	ATGACTCTACCCACGGCAAG	GATCTCGCTCCTGGAAGATG

the lysate was centrifuged at 12,000×*g* for 20 min at 4 °C to extract the total protein. The nuclear and cytoplasmic proteins were extracted using the nuclear/cytoplasmic isolation kit (P1201, APPLYGEN, China) following the manufacturer's guidelines. The protein concentration was determined using a BCA Protein Assay Kit (P1511, APPLYGEN, China). Following our previous descriptions[40], we performed Western blot using sodium dodecyl sulfate polyacrylamide gel electrophoresis (SDS-PAGE). Then the membranes were incubated overnight at 4 °C with the following primary antibodies: mouse anti-TH antibody (1:1000, MAB318, Millipore), mouse anti-TLR4 antibody (1:400, ab22048; Abcam, Cambridge, MA, USA), mouse anti phosphorylated-IκB-α (1:400, sc-8404; Santa Cruz Biotechnology Inc., Santa Cruz, CA, USA), rabbit anti-IκB-α (1:400, sc-371; Santa Cruz Biotechnology Inc., Santa Cruz, CA, USA), rabbit anti-NF-κB P65 antibody (1:1000, A2547, Abclonal, China), rabbit anti-MyD88 (1:400, ab2064; Abcam, Cambridge, MA, USA), rabbit anti-ZO-1 antibody (1:1000, ab96587, Abcam), rabbit anti-occludin antibody (1:1000, 27260-1-AP, ProteinTech), mouse anti-claudin-1 antibody (1:1000, 2H10D10, Invitrogen), mouse anti-claudin-5 antibody (1:1000, A10207, Abclonal, China). The membranes were then incubated with corresponding secondary antibody (AS014, 1:2000, Abclonal, China) for 2 h at room temperature. The blots were developed with LAS4000 chemiluminescence system (Fujifilm, Tokyo, Japan), and the densities of the bands were determined by Gel-Pro Analyzer 4.0 software.

2.16. *Statistical analysis*

We conducted the statistical analysis using SPSS version 20.0 software. Data were presented as the mean ± standard deviation (SD). Multiple comparisons were performed by one-way analysis of variance, followed by the least significant difference test. For pole test, hanging grip test and ZO-1 integrity scores and cell numbers, the Kruskal−Wallis test was used, followed by the Mann−Whitney U test. The independent *t* test was applied to two-group comparisons. P values < 0.05 were considered statistically significant.

3. Results

3.1. *FLZ treatment alleviates weight loss and motor dysfunctions of the rotenone-induced PD mice*

Body weight loss and motor dysfunctions are commonly witnessed in PD animal models. To assess the neuroprotective effects of FLZ treatment, mice were administrated with rotenone for four weeks to induce the PD model. Then, 15 randomly selected mice were treated with FLZ in the following two weeks (Fig. 1B). In the first 4 weeks, the Model group showed significantly lower body weight than the Control group (Fig. 1C). In the following 2 weeks, FLZ treatment remarkably attenuated the body weight loss (Fig. 1D). Additionally, 4 different behavioral experiments including the rotarod test for motor coordination impairment (Fig. 1E and F), the adhesive removal test for motor and sensory impairment (Fig. 1G and H), the hanging grip test for muscle strength (Fig. 1I and J), and the pole test for bradykinesia (Fig. 1K and L) were carried out at three different time points (Weeks 3, 4 and 6; Fig. 1B). The Model group exhibited significantly reduced time on the rod ($P < 0.001$, Fig. 1E), longer time to remove the stickers ($P < 0.001$, Fig. 1G), lower scores of muscle strength ($P < 0.001$, Fig. 1I) and decreased performance scores in the pole test ($P < 0.001$, Fig. 1K) from Week 4. However, there were no significant differences between the Control and Model groups at Week 3 (Fig. 1E, G, I and K). After FLZ administration for 2 weeks, the FLZ group showed remarkable improvement in the rotarod test ($P < 0.01$, Fig. 1F), the adhesive removal test ($P < 0.001$, Fig. 1H), the hanging grip test ($P < 0.001$, Fig. 1J) and the pole test ($P < 0.001$, Fig. 1L) compared to the Rotenone group. Together, these results indicate that rotenone administration causes motor deficits in mice from Week 4 and FLZ treatment alleviates weight loss and motor deficits induced by oral rotenone administration.

3.2. *FLZ treatment improves GI dysfunctions of the rotenone-induced mouse model*

Expect for motor dysfunctions, the mouse model challenged by rotenone also recapitulates some aspects of GI dysfunctions

associated with PD. The distance travelled by Evans blue dye in the intestinal tract was used as a GI parameter to evaluate the effect of FLZ treatment. Rotenone exposure significantly delayed intestinal transit (indicated by decreased Evans blue transit distance) at Week 3 ($P < 0.05$) and Week 4 ($P < 0.01$) (Fig. 2A) compared to the Control group whereas FLZ treatment remarkably improved the reduced intestinal transit at Week 6 ($P < 0.05$) (Fig. 2B). Correspondingly, the rotenone-induced mice exhibited a reduction in colon length since Week 3 (Week 3, $P < 0.01$; Week 4, $P < 0.001$; Week 6, $P < 0.001$) compared to the vehicle-treated mice (Fig. 2C and D). Meanwhile, FLZ treatment remarkably alleviated the reduction in colon length at Week 6 ($P < 0.001$) (Fig. 2D). Furthermore, we assessed colon motility and found that fecal water content (Week 3-Week 6, all $P < 0.001$) and fecal pellet output (Week 3-Week 6, all $P < 0.001$) significantly decreased after 3 weeks of rotenone exposure (Fig. 2E−H). In contrast, the FLZ group displayed remarkably increased percentage of water content as well as fecal pellet output at Week 5 (water content percentage, $P < 0.001$; fecal pellet output, $P < 0.05$) and Week 6 (both $P < 0.001$) (Fig. 2F and H). Furthermore, there were significant differences in colon motility as evaluated by 20 min stool collection between rotenone and vehicle-treated mice from Week 3 to Week 6 (Fig. 2I−L). Fecal pellet output frequency was remarkably increased in the FLZ group as compared to the Rotenone group at Week 6 (Fig. 2L). These data suggest that rotenone-induced mice start to show GI dysfunctions from Week 3, which are prior to the motor symptoms and can be alleviated by FLZ treatment.

3.3. FLZ treatment restores dopaminergic neuronal deficits via reducing neuroinflammation in the SN

The dopaminergic neuronal deficits caused by neuroinflammation in the SN region play an important role in the development of motor dysfunctions. The activation of brain glial cells, including microglia and astrocytes, contributes to the neuroinflammation in PD pathogenesis[41,42]. Hence, to evaluate the neuroprotective effects of FLZ administration, we examined the correlation of glial cells and dopaminergic neurons using immunofluorescence staining. The SN region was immunostained with Iba-1 as the microglial marker, GFAP as the astrocyte marker, and TH as the marker of dopaminergic neurons. The results of immunofluorescence staining reveal a significant reduction of TH^+ dopaminergic neurons by about 50% in the Rotenone group compared to the Control group ($P < 0.001$), which was significantly alleviated by FLZ treatment ($P < 0.001$) (Fig. 3A, B, E and F). Accordingly, the Western blot results illustrate that rotenone administration suppressed the expression of TH in the SN ($P < 0.01$). However, FLZ treatment reversed this reduction in rotenone-induced mice ($P < 0.001$) (Fig. 3I and J). As shown in Fig. 3A and D, the number of $GFAP^+$ astrocytes were remarkably increased in the SN region of Rotenone group ($P < 0.001$), while FLZ treatment significantly attenuated the elevation (Rotenone group, 28 cells; FLZ group, 14 cells; $P < 0.001$). Similarly, as illustrated in Fig. 3E and H, there were more Iba-1^+ cells in the SN of the Rotenone group compared to the Control group ($P < 0.001$). However, after FLZ administration, Iba-1^+

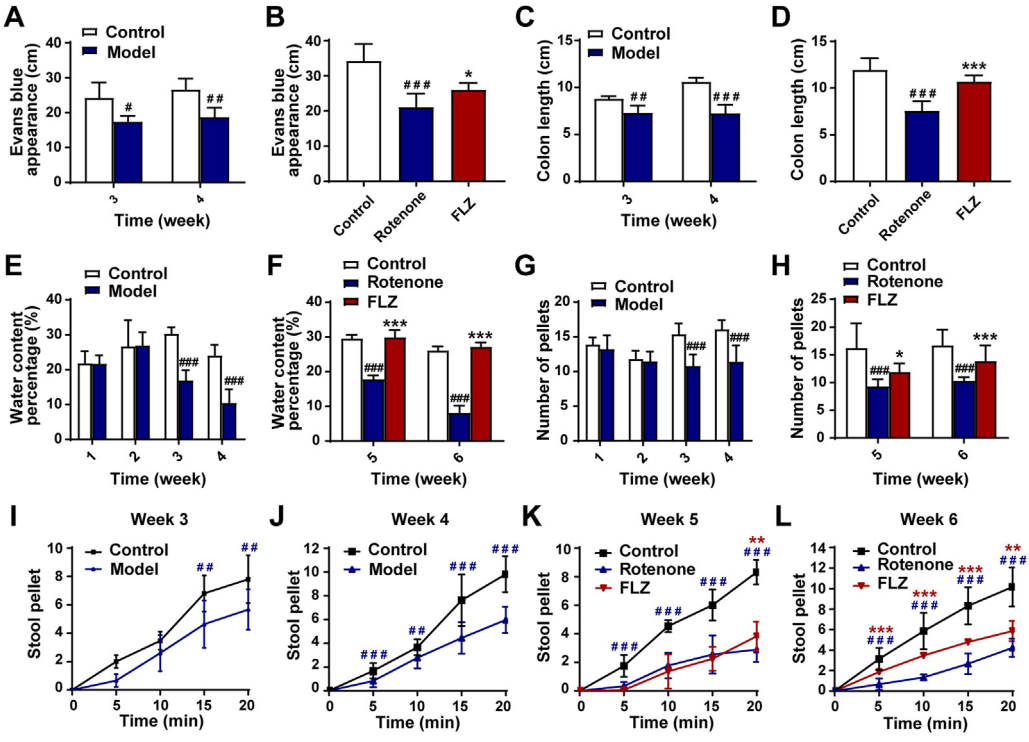

Figure 2 FLZ treatment improves GI dysfunctions of the rotenone PD mouse model. (A) and (B) Intestinal transit distance in Weeks 3−4 (A) and Week 6 (B). (C)−(D) Colon length in Weeks 3−4 (C) and Week 6 (D). (E)−(F) Water percentage in fecal pellets in Weeks 1−4 (E) and Weeks 5−6 (F). (G)−(H) Numbers of total fecal pellets in Weeks 1−4 (G) and Weeks 5−6 (H). (I)−(L) Time course of fecal output over 20 min in Weeks 3−6. In (A)−(D), $n = 5$ replicates in each group. For GI function tests in Weeks 1−4, $n = 15$ for the Control group; $n = 30$ for the Model group. For GI function tests in Weeks 5−6, $n = 15$ for each group. Data are presented as mean ± SD. $^{\#}P < 0.05$, $^{\#\#}P < 0.01$, $^{\#\#\#}P < 0.001$ *versus* the Control group; $^{*}P < 0.05$, $^{**}P < 0.01$, $^{***}P < 0.001$ *versus* the Rotenone group.

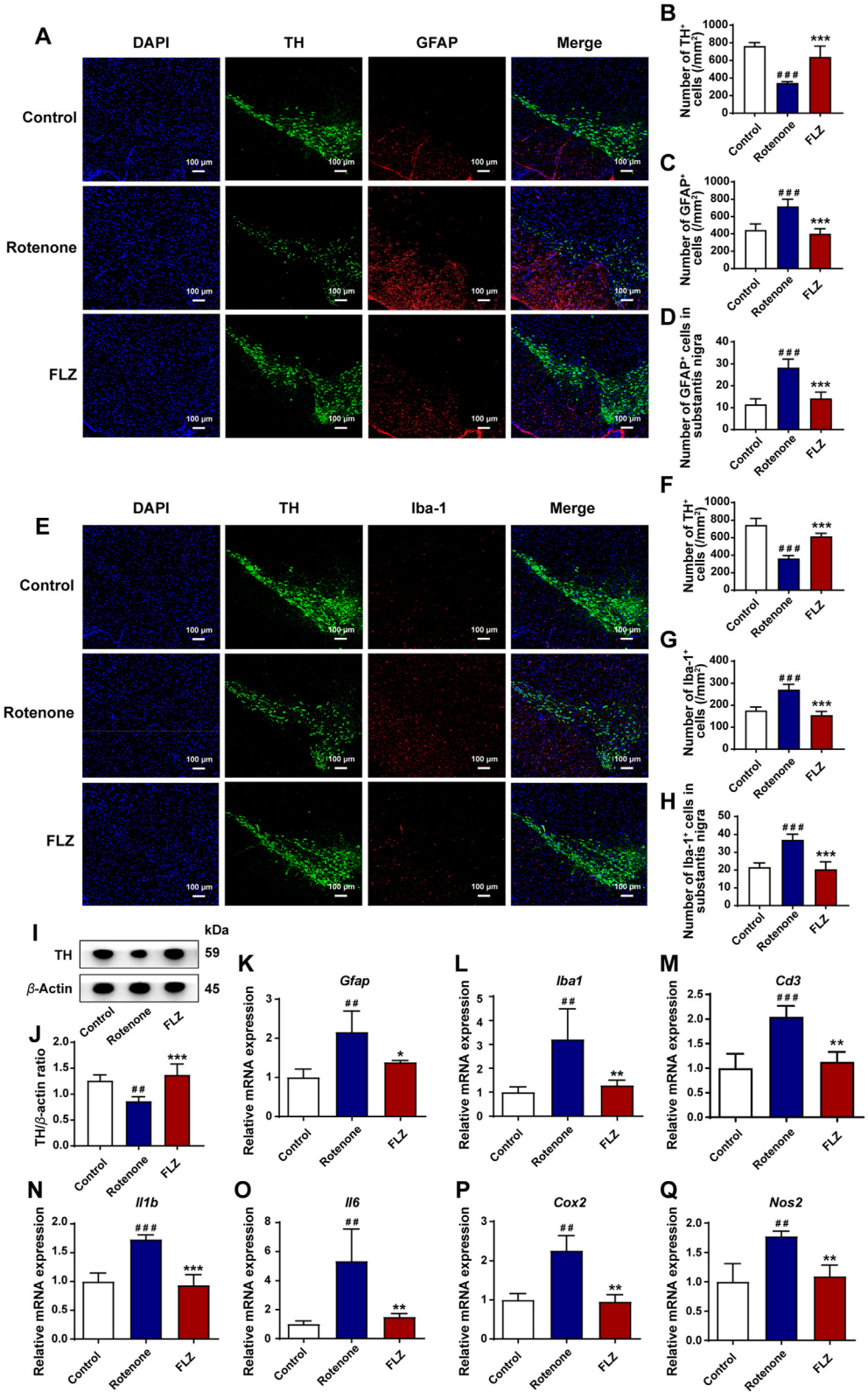

Figure 3 FLZ treatment restores dopaminergic neuronal deficits *via* reducing neuroinflammation in the SN. (A) Representative captures of immunofluorescence in the SN of nuclei (DAPI, blue), total dopaminergic neurons (TH, green), and astrocytes (GFAP, red). (B)−(D) Numbers of TH^+ cells (B), $GFAP^+$ cells (C) and $GFAP^+/TH^+$ cells (activated astrocytes in SN) (D). (E) Representative captures of immunofluorescence in the SN of nuclei (DAPI, blue), total dopaminergic neurons (TH, green), and microglial cells (Iba-1, red). (F)−(H) Numbers of TH^+ cells (F), Iba-1^+ cells (G) and Iba-$1^+/TH^+$ cells (activated microglial cells in SN) (H). (I) Representative western blot brands of TH in SN. (J) The density analysis result of TH Western blot in SN. (K)−(L) mRNA expression of glial cell markers *Gfap* and *Iba1*, as well as (M)−(Q) neuroinflammatory markers (*Cd3*, *Il1b*, *Il6*, *Cox 2*, and *Nos 2*) in SN. In (B)−(D) and (F)−(H), $n = 5$ for each group. In (J), $n = 4$ for each group. In (K)−(Q), $n = 3$ for each group. Data are presented as mean ± SD. $^{\#\#}P < 0.01$, $^{\#\#\#}P < 0.001$ *versus* the Control group; $^{*}P < 0.05$, $^{**}P < 0.01$, $^{***}P < 0.001$ *versus* the Rotenone group.

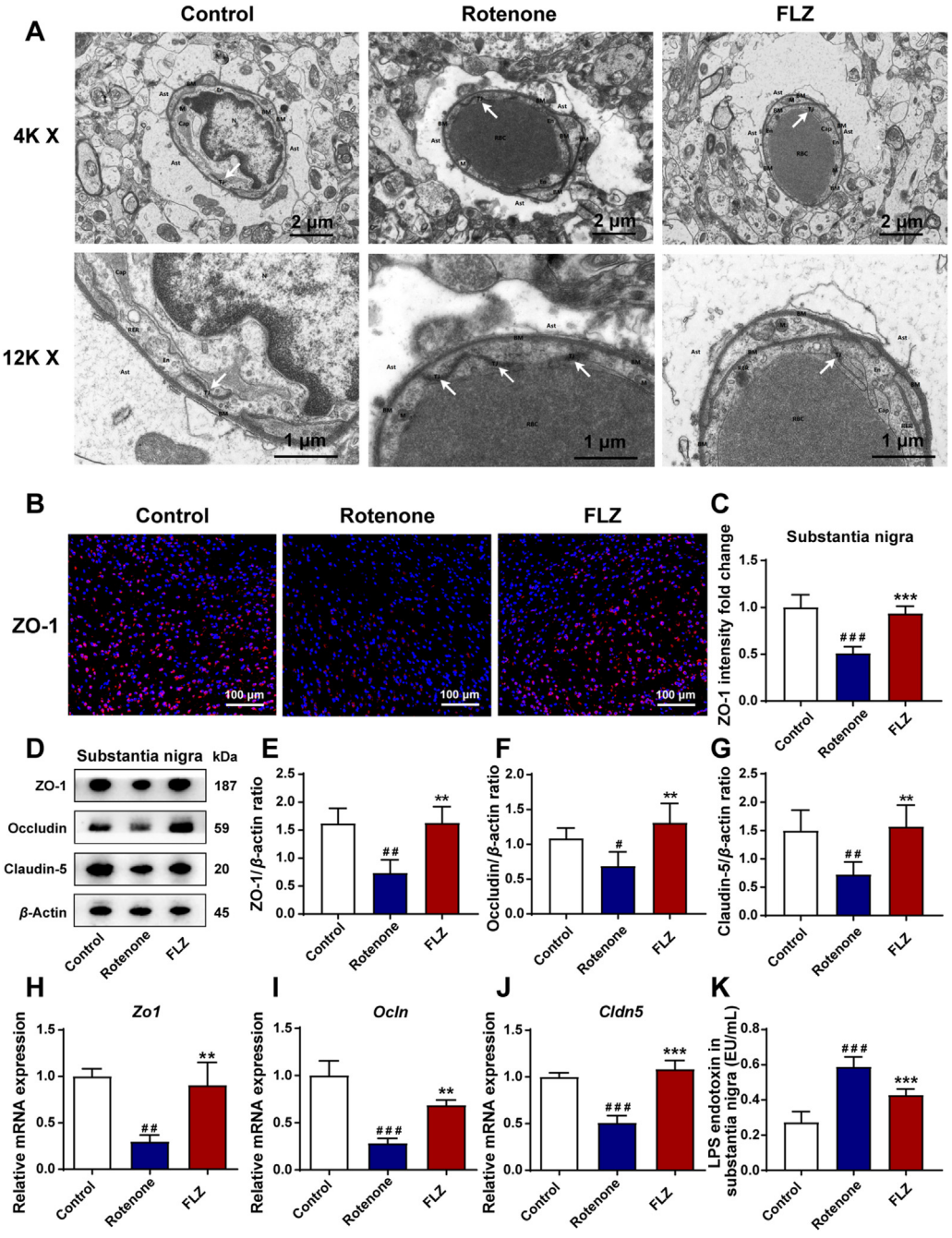

Figure 4 FLZ administration attenuates BBB impairment caused by rotenone. (A) Representative electron micrographs showing the tight junction structure of BBB. (B) Representative captures of immunofluorescence of ZO-1 in the SN. (C) The intensity analysis of ZO-1 immunofluorescence staining. (D) Representative Western blot brands of ZO-1, occludin and claudin-5 in SN. (E)−(G) The density analysis results of ZO-1, occludin and claudin-5 Western blot in SN. (H)−(J) mRNA expression of tight junction proteins *Zo1*, *Ocln* and *Cldn5*. (K) Levels of LPS endotoxin in the SN. In (C), $n = 5$ for each group. In (E)−(G), $n = 4$ for each group. In (H)−(J), $n = 3$ for each group. In (K), $n = 8$ for each group. Data are presented as mean ± SD. $^{\#}P < 0.05$, $^{\#\#}P < 0.01$, $^{\#\#\#}P < 0.001$ *versus* the Control group; $^{**}P < 0.01$, $^{***}P < 0.001$ *versus* the Rotenone group.

microglia were markedly decreased (Rotenone group, 37 cells; FLZ group, 20 cells; $P < 0.001$) (Fig. 3H). Consistent with the immunofluorescence staining results, the mRNA expression of *Gfap* and *Iba1* levels was elevated in the Rotenone group (both $P < 0.01$) and reduced by FLZ administration (*Gfap*, $P < 0.05$; *Iba1*, $P < 0.01$) (Fig. 3K and L). To further characterize the inflammatory status in the SN, we tested the expression of related proteins by qPCR. The levels of neuroinflammatory markers including *Cd3* ($P < 0.001$), *Il1b* ($P < 0.001$), *Il6* ($P < 0.01$), *Cox 2* ($P < 0.01$), and *Nos 2* ($P < 0.01$) increased remarkably in the Rotenone group and declined significantly in the FLZ group (*Cd3*, $P < 0.01$; *Il1b*, $P < 0.001$; *Il6*, $P < 0.01$; *Cox2*, $P < 0.01$; *Nos2*, $P < 0.01$) (Fig. 3M−Q). Taken together, these results demonstrate that FLZ treatment suppresses the loss of dopaminergic neurons *via* reducing neuroinflammation in the SN.

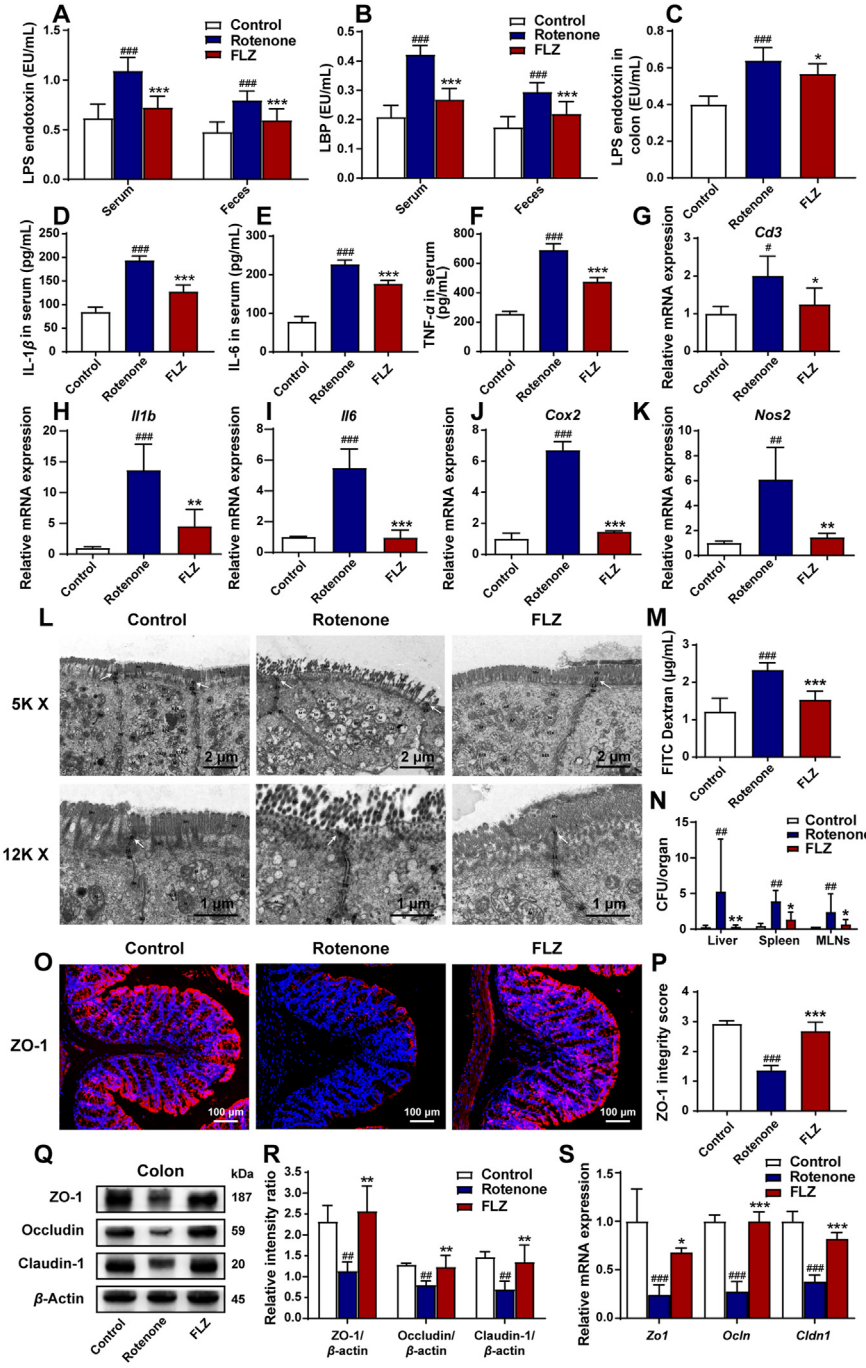

Figure 5 FLZ administration attenuates systemic inflammation caused by increased intestinal inflammation and permeability in the rotenone-induced mouse model. (A)−(F) Levels of LPS endotoxin in the serum and feces. (B) Levels of LBP in the serum and feces. (C) Levels of LPS endotoxin in the colon. (D)−(F) Serum levels of IL-1β, IL-6, and TNF-α. (G)−(K) The mRNA expression of inflammatory markers (*Cd3*, *Il1b*, *Il6*, *Cox 2*, and *Nos 2*) in the colon. (L) Representative electron micrographs showing the tight junction structure of intestinal epithelium in the colon. (M) Concentrations of FITC in serum showing intestinal permeability. (N) Number of bacteria (CFUs) in the liver, spleen, and MLNs. (O) Representative captures of immunofluorescence in the colon of ZO-1. (P) ZO-1 integrity score in the colon. (Q) Representative Western blot brands of ZO-1, occludin and claudin-1 in the colon. (R) The density analysis results of ZO-1, occludin and claudin-1 Western blot in the colon. (S) The mRNA expression of tight junction proteins *Zo1*, *Ocln* and *Cldn1* in the colon. In (A)−(F), $n = 8$ for each group. In (G)−(K), $n = 3$ for each group. In (M) and (P), $n = 5$ for each group. In (N), $n = 6$ for each group. In (R), $n = 4$ for each group. In (S), $n = 3$ for each group. Data are presented as mean ± SD. $^{\#}P < 0.05$, $^{\#\#}P < 0.01$, $^{\#\#\#}P < 0.001$ *versus* the Control group; $^{*}P < 0.05$, $^{**}P < 0.01$, $^{***}P < 0.001$ *versus* the Rotenone group.

3.4. FLZ treatment improves BBB impairment caused by rotenone

Evidence has illustrated that the BBB impairment may lead to neuroinflammation and subsequent dopaminergic neuronal death in PD pathogenesis[43]. Tight junction is a critical functional unit for the maintenance of the BBB permeability. Therefore, the TEM analysis was performed to investigate the ultrastructure of tight junction in the SN. As shown in Fig. 4A, the tight junctions in the Rotenone group demonstrated a disorganized and diffuse structure as well as severe local endothelial damage compared to the Control group. However, the structure of tight junction was significantly improved with clarity and integrity by FLZ treatment. Besides, the damage of endothelial cells and surrounding brain tissues was also alleviated. ZO-1 is a key component of the tight junction initially identified in the BBB[43]. Its expression and distribution in the SN were determined by immunofluorescence staining. The results showed a statistically significant reduction of ZO-1 expression to almost a half in the Rotenone group compared to the Control group ($P < 0.001$) while the expression of ZO-1 was significantly improved in the FLZ group ($P < 0.001$) (Fig. 4B and C). Next, we detected the expression of three major tight junction proteins including ZO-1, occludin, and claudin-5 by Western blot in the SN region. Remarkably lower expression of ZO-1 ($P < 0.01$), occludin ($P < 0.05$), and claudin-5 ($P < 0.01$) than the Control group was observed in the Rotenone group (Fig. 4D−G). In contrast, FLZ administration restored the expression of the three tight junction associated proteins (all $P < 0.01$) (Fig. 4D−G). Consistently, the mRNA expression of *Zo1* ($P < 0.01$), *Ocln* ($P < 0.001$), and *Cldn5* ($P < 0.001$) was also decreased in the Rotenone group compared to the Control group (Fig. 4H−J). While, treatment with FLZ markedly preserved the mRNA expression of these proteins (*Zo1*, $P < 0.01$; *Ocln*, $P < 0.01$; *Cldn5*, $P < 0.001$) (Fig. 4H−J). As a result of the impaired BBB function in the rotenone-challenged mice, the increased LPS levels were detected by ELISA in the SN of the Rotenone group mice compared to the Control group mice ($P < 0.001$). However, FLZ treatment remarkably suppressed the LPS levels in the SN (Rotenone group, 0.59 EU/mL; FLZ group, 0.43 EU/mL; $P < 0.001$) (Fig. 4K). These findings indicate that FLZ treatment improves the BBB impairment caused by rotenone, contributing to the alleviation of neuroinflammation.

3.5. FLZ treatment attenuates systemic inflammation caused by increased intestinal inflammation and permeability in the rotenone-induced mouse model

In the pathogenesis of PD, the BBB impairment may be caused by increased pro-inflammatory cytokines and pathogens (like LPS and bacteria) in the systemic circulation. Besides, the leakage of pro-inflammatory factors into the blood and the occurrence of systemic inflammation may stem from intestinal inflammation and the damaged gut barrier integrity and function[20]. Hereby, we detected the levels of LPS, LBP, and pro-inflammatory cytokines in the serum. What's more, we measured the intestinal inflammation and permeability using various approaches. ELISA results showed that the Rotenone group had approximately twice higher levels of serum LPS and serum LBP than the Control group (both $P < 0.001$) (Fig. 5A−B). However, the FLZ group illustrated remarkably lower levels of LPS (Rotenone group, 1.09 EU/mL; FLZ group, 0.73 EU/mL; Fig. 5A) and LBP (Rotenone group, 0.42 EU/mL; FLZ group, 0.27 EU/mL; Fig. 5B) in the serum than the Rotenone group (both $P < 0.001$). To further evaluate the systemic inflammation status, we assessed the levels of three pro-inflammatory cytokines in the serum of different groups using ELISA analysis. All the three cytokines (IL-1β, IL-6, and TNF-α) in the Rotenone group increased more than two times compared to the Control group (all $P < 0.001$), while the levels of these three pro-inflammatory cytokines markedly declined in the FLZ group (all $P < 0.001$) (Fig. 5D−F). These data collectively support that FLZ treatment can suppress the systemic inflammation in the rotenone-challenged mice.

In addition to the systemic inflammation, the intestinal inflammation was also assessed in the study. Consistent with the levels of LPS and LBP in the serum, the LPS levels in the colon also remarkably increased in the Rotenone group compared to the Control group ($P < 0.001$) whereas FLZ treatment reduced the LPS levels (Rotenone group, 0.64 EU/mL; FLZ group, 0.57 EU/mL; $P < 0.05$) (Fig. 5C). Besides, ELISA analysis revealed that fecal LPS and LBP also elevated in the Rotenone group compared to the Control group (both $P < 0.001$), while FLZ administration decreased the levels of LPS (Rotenone group, 0.80 EU/mL; FLZ group, 0.59 EU/mL; Fig. 5A) and LBP (Rotenone group, 0.30 EU/mL; FLZ group, 0.22 EU/mL; Fig. 5B) in the feces (both $P < 0.001$; Fig. 5A and B). Further qPCR analysis of intestinal inflammatory status revealed the increased mRNA expression of inflammatory factors, including *Cd3* ($P < 0.05$), *Il1b* ($P < 0.001$), *Il6* ($P < 0.001$), *Cox 2* ($P < 0.001$), and *Nos 2* ($P < 0.01$) in the Rotenone group. Notably, reduced mRNA expression was observed in the FLZ group (*Cd3*, $P < 0.05$; *Il1b*, $P < 0.01$; *Il6*, $P < 0.001$; *Cox2*, $P < 0.001$; *Nos2*, $P < 0.01$) (Fig. 5G−K). These results support that FLZ administration can inhibit the intestinal inflammation caused by rotenone as well.

To determine whether the damaged intestinal barrier linked the systemic inflammation with intestinal inflammation, experiments were conducted to measure the intestinal permeability and barrier structure. TEM analysis was utilized to show the intestinal barrier structures in different groups. As demonstrated in Fig. 5L, the Control group mice had an intact epithelium and regular brush border whereas the Rotenone group mice showed a damaged, fragmented epithelium with some short villi in enterocytes and wider intercellular gaps. In the Rotenone group, the decreased electron-dense materials between the adjacent cells near the epithelium indicated the destruction of tight junction structure. In contrast, FLZ treatment prevented the damage of epithelium as well as tight junctions in rotenone-intoxicated mice. To further evaluate the gut permeability in different groups, we conducted FITC *in vivo* assays. The concentration of FITC in serum remarkably increased in the Rotenone group compared to the Control group ($P < 0.001$) whereas FLZ administration significantly attenuated the elevation of FITC concentration in the serum ($P < 0.001$) (Fig. 5M). At sacrifice, remarkable bacterial growth was detected in the livers, spleens, and MLNs of the Rotenone group compared to the Control group (all $P < 0.01$). In contrast, FLZ treatment significantly inhibited the bacterial translocation (liver, $P < 0.01$; spleen, $P < 0.05$; MLNs, $P < 0.05$) (Fig. 5N). These results suggest that FLZ treatment attenuates intestinal barrier induced by rotenone.

Tight junction plays a critical role in the integrity of intestinal barrier. To further evaluate the function of tight junctions among different groups, we detected three main proteins (ZO-1, occludin and claudin-1) by immunofluorescence staining, Western blot, and qPCR analysis. By immunofluorescence staining, continuous structure and robust expression of ZO-1 were shown at the

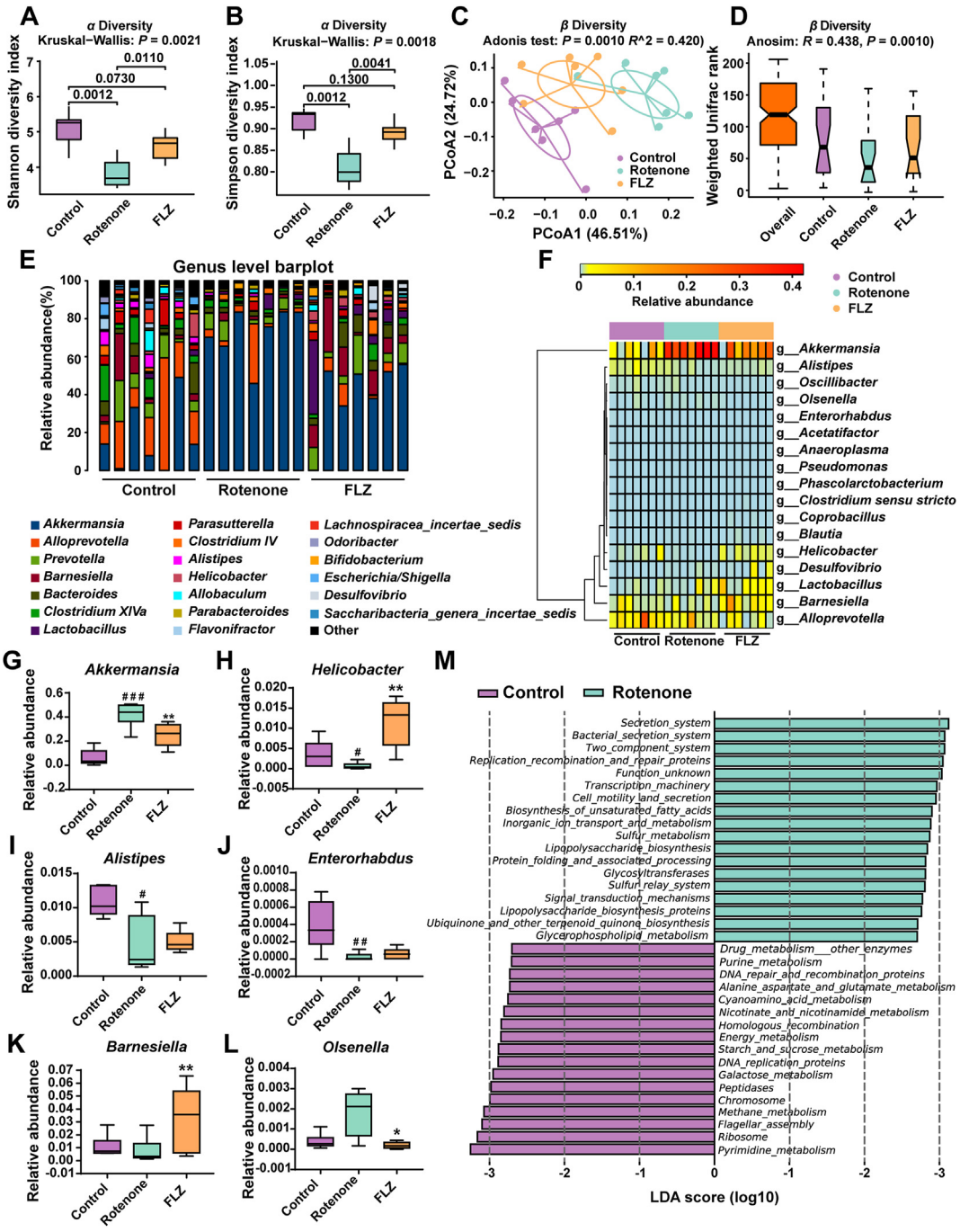

Figure 6 FLZ treatment alleviates gut microbiota dysbiosis of the rotenone-induced PD mice. (A) Analysis of alpha diversity of gut microbiota by Shannon analysis. (B) Analysis of alpha diversity of gut microbiota by Simpson analysis. (C) PCoA plots of beta diversity based on weighted UniFrac Adonis analysis in different groups. (D) Beta diversity based on weighted UniFrac ANOSIM analysis in different groups. (E) Relative abundance of gut microbiota at the genus level in the three groups. (F) Heatmap analysis of relative abundance of gut microbiota at the genus level in different groups. (G)−(L) Relative abundance of six significantly altered bacterial genera: *Akkermansia*, *Helicobacter, Alistipes*, *Enterorhabdus*, *Barnesiella*, *Olsenella.* (M) Bar graph of LDA score of enriched KEGG pathways at level 3. LDA scores (log 10) > 2.7 and $P < 0.05$ are shown. In this figure, $n = 7$ for each group. Each boxplot represents the median, interquartile range, minimum and maximum values. $^{\#}P < 0.05$, $^{\#\#}P < 0.01$, $^{\#\#\#}P < 0.001$ *versus* the Control group; $^{*}P < 0.05$, $^{**}P < 0.01$ *versus* the Rotenone group.

epithelial lining of the Control group, while the Rotenone group showed discontinuous staining and light fluorescence (Fig. 5O). Integrity scoring scale analysis demonstrated remarkably reduced expression and destroyed structure of ZO-1 in the Rotenone group ($P < 0.001$) while FLZ treatment significantly restored the ZO-1 integrity to almost the twice of the Rotenone group ($P < 0.001$) (Fig. 5P). In addition, Western blot illustrated markedly lower expression of ZO-1, occludin, and claudin-1 (all $P < 0.01$) in the colonic samples of the Rotenone group than the Control group (Fig. 5Q and R). However, FLZ administration significantly attenuated the loss of these three proteins (all $P < 0.01$) (Fig. 5Q and R). Consistently, the mRNA expression of *Zo1*, *Ocln*, and

Cldn1 remarkably decreased in the Rotenone group in comparison with the Control group (all $P < 0.001$) (Fig. 5S), while FLZ treatment significantly increased the mRNA expression of *Zo1* ($P < 0.05$), *Ocln* ($P < 0.001$), and *Cldn1* ($P < 0.001$) (Fig. 5S). All the results in this part suggest that FLZ administration alleviates the increased intestinal inflammation and permeability triggered by rotenone, thus inhibiting the systemic inflammation.

3.6. FLZ treatment alleviates gut microbiota dysbiosis of the rotenone-induced PD mice

It is acknowledged that altered microbiota composition is closely related to the development of PD[44]. Hence, we collected the fecal pellets at Week 4 for microbiota analysis, which revealed that the microbiota community of the Model group mice was already separated from the Control group mice. Also, several bacterial taxa at various levels exerted different abundances between these two groups, including Verrucomicrobia phylum and *Akkermansia* genus. To further validate our hypothesis that FLZ treatment inhibited intestinal inflammation by alleviating the gut microbiota dysbiosis in rotenone-challenged mice, we detected gut microbiota composition of mice from three different groups at Week 6. First of all, the analysis based on alpha and beta diversity was performed. In Fig. 6A and B, alpha diversity analysis showed that Rotenone group had significantly decreased community richness and diversity compared to the Control group (Shannon index: $P = 0.0012$; Simpson index: $P = 0.0012$), while the FLZ group demonstrated significantly higher richness and diversity than the Rotenone group (Shannon index: $P = 0.0110$; Simpson index: $P = 0.0041$). PCoA based on weighted UniFrac distances was utilized to measure beta diversity. Adonis analysis revealed that the gut microbial community was significantly separated among three groups ($R = 0.420$; $P = 0.0010$) (Fig. 6C) and ANOSIM showed consistent results ($R = 0.438$; $P = 0.0010$) (Fig. 6D).

To further explore how the microbiota structure changed between groups, relative abundance at phylum, family and genus levels was displayed and analyzed. At the phylum level, Bacteroidetes, Firmicutes, and Verrucomicrobia dominated the microbial community (Supporting Information Fig. S1A) while Porphyromonadaceae, Verrucomicrobiaceae, and Lachnospiraceae were the most abundant families (Fig. S1B). Additionally, fecal microbial distribution across all the samples at genus level is illustrated in Fig. 6E. All the phyla, families, and genera with relative abundance over 0.01% and significant differences ($P < 0.05$) among groups were displayed in Table 2. Alterations of fecal microbes among three groups were observed in three phyla, including Verrucomicrobia ($P = 0.0009$), Proteobacteria ($P = 0.0179$), and Bacteroidetes ($P = 0.0399$) (Table 2). Compared to the Control group, increased phylum Verrucomicrobia ($P = 0.0006$), decreased phyla Proteobacteria ($P = 0.0407$) and Bacteroidetes ($P = 0.0262$) were detected in the Rotenone group (Table 2). However, FLZ treatment reversed the changes in these phyla (Verrucomicrobia, $P = 0.0070$; Proteobacteria, $P = 0.0105$; Bacteroidetes, $P = 0.0379$) (Table 2). At the family taxonomic level, we found increased relative abundance in Verrucomicrobiaceae ($P = 0.0006$) and declined relative abundance in Helicobacteraceae ($P = 0.0297$), Rikenellaceae ($P = 0.0111$), as well as Porphyromonadaceae ($P = 0.0111$) in the Rotenone group compared to the Control group (Table 2). The opposite trends of these families, except Rikenellaceae which showed no significant differences, were found when comparing the FLZ group with the Rotenone group (Verrucomicrobiaceae, $P = 0.0070$; Helicobacteraceae, $P = 0.0026$; Porphyromonadaceae, $P = 0.0175$) (Table 2).

Significantly different species at the genus level among these three groups were summarized in a heatmap (Fig. 6F) and six of them were illustrated as boxplots (Fig. 6G−L). In comparison with the Control group, genera *Akkermansia* ($P = 0.0006$) (Fig. 6G) and *Olsenella* (Fig. 6L) had higher relative abundance while genera *Helicobacter* ($P = 0.0297$) (Fig. 6H), *Alistipes* ($P = 0.0111$) (Fig. 6I), and *Enterorhabdus* ($P = 0.0094$) (Fig. 6J) had significantly lower abundance in the Rotenone group.

Table 2 Relative abundance of microbial taxa in different groups.

Taxonomic level	Relative abundance			*P*-value		
	Control	Rotenone	FLZ	Overall	Con *vs.* Rot	Rot *vs.* FLZ
Phylum						
Verrucomicrobia	0.0388	0.3405	0.1650	0.0009	$0.0006^{\#\#\#}$	0.0070**
Proteobacteria	0.0261	0.0081	0.0238	0.0179	$0.0407^{\#}$	0.0105*
Bacteroidetes	0.6093	0.4203	0.5817	0.0399	$0.0262^{\#}$	0.0379*
Family						
Verrucomicrobiaceae	0.0388	0.3405	0.1650	0.0009	$0.0006^{\#\#\#}$	0.0070**
Helicobacteraceae	0.0058	0.0005	0.0086	0.0029	$0.0297^{\#}$	0.0026**
Rikenellaceae	0.0086	0.0034	0.0035	0.0045	$0.0111^{\#}$	0.6200
Porphyromonadaceae	0.4929	0.3569	0.5135	0.0174	$0.0111^{\#}$	0.0175*
Genus						
Akkermansia	0.0388	0.3405	0.1650	0.0009	$0.0006^{\#\#\#}$	0.0070**
Helicobacter	0.0058	0.0005	0.0086	0.0029	$0.0297^{\#}$	0.0026**
Alistipes	0.0086	0.0034	0.0034	0.0045	$0.0111^{\#}$	0.6200
Enterorhabdus	0.0003	0.0000	0.0000	0.0093	$0.0094^{\#\#}$	0.3186
Barnesiella	0.0142	0.0060	0.0457	0.0152	0.2086	0.0041**
Oscillibacter	0.0018	0.0012	0.0003	0.0176	0.3706	0.0398*
Desulfovibrio	0.0001	0.0011	0.0063	0.0221	$0.0045^{\#\#}$	0.4428
Alloprevotella	0.0721	0.0277	0.0133	0.0253	$0.0379^{\#}$	0.3829
Olsenella	0.0007	0.0012	0.0002	0.0328	0.1788	0.0146*

$^{\#}P < 0.05$, $^{\#\#}P < 0.01$, $^{\#\#\#}P < 0.001$ *versus* the Control group; $^{*}P < 0.05$, $^{**}P < 0.01$ *versus* the Rotenone group. Statistical analysis by Kruskal−Wallis multiple comparison test with *post-hoc* Mann−Whitney U test.

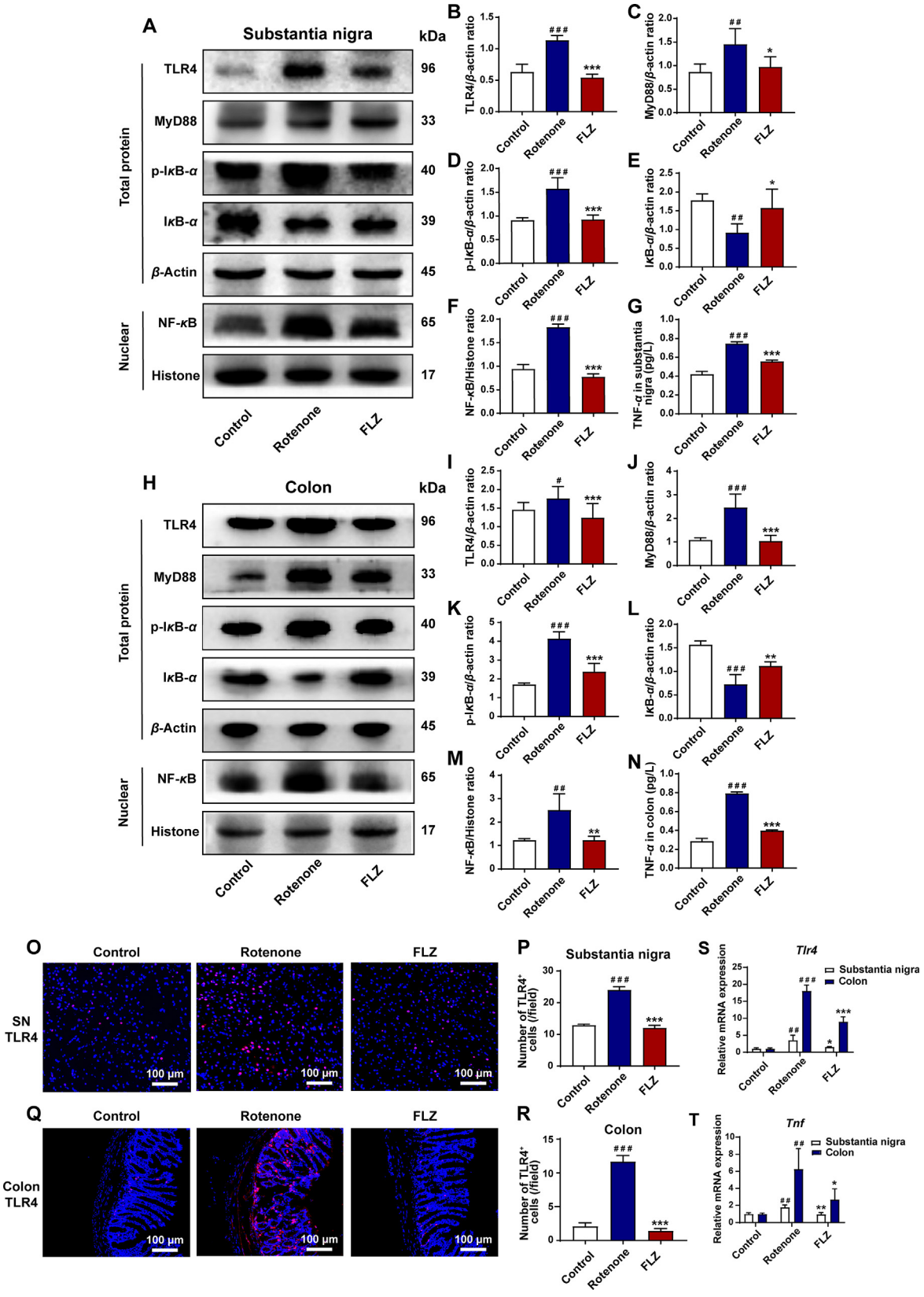

Figure 7 FLZ administration inhibits intestinal inflammation and neuroinflammation by inhibiting TLR4/MyD88/NF-κB signaling pathway. (A) Representative Western blot brands of TLR4, MyD88, p-IκB-α, IκB-α, and NF-κB in SN. (B)−(F) The density analysis results of TLR4, MyD88, p-IκB-α, IκB-α, and NF-κB in SN. (G) ELISA levels of TNF-α in SN. (H) Representative Western blot brands of TLR4, MyD88, p-IκB-α, IκB-α, and NF-κB in colon. (I)−(M) The density analysis results of TLR4, MyD88, p-IκB-α, IκB-α, and NF-κB in colon. (N) ELISA levels of TNF-α in colon. (O) Representative captures of immunofluorescence of TLR4 in SN. (P) Numbers of $TLR4^+$ cells in SN. (Q) Representative captures of immunofluorescence of TLR4 in colon. (R) Numbers of $TLR4^+$ cells in colon. (S) The mRNA expression of *Tlr4* in SN and colon. (T)

However, FLZ treatment decreased abundance of *Akkermansia* ($P = 0.0070$) (Fig. 6G) and *Olsenella* ($P = 0.0146$) (Fig. 6L) whereas elevated relative abundance of *Helicobacter* ($P = 0.0026$) (Fig. 6H) and *Barnesiella* ($P = 0.0041$) (Fig. 6K) was observed in the FLZ group.

In addition, functional analysis identified a total of 23 KEGG pathways at level 2 (Fig. S1C). Replication and repair, translation, and nucleotide metabolism pathways were enriched in the Control group. Meanwhile, pathways including lipid metabolism, cellular processes and signaling, and xenobiotics biodegradation and metabolism were enriched in the Rotenone group. Besides, increased abundance in circulatory system and neurodegenerative diseases pathways was predicted in the FLZ group (Fig. S1C). Additionally, level 3 analysis inferred that 17 pathways, including pyrimidine metabolism, ribosome, and energy metabolism pathways, enriched in the Control group (Fig. 6M). In addition, there were 21 Level 3 pathways enriched in the Rotenone group, including secretion system, bacterial secretion system, two component system, replication recombination and repair proteins, and lipopolysaccharide biosynthesis (Fig. 6M). To prove the correlation between microbiota and neuroinflammation, we calculated the correlations between the abundances of differential microbial genera and neuroinflammation-related data. The results reveal that microbial community in the feces strongly correlates with neuroinflammation of PD (glial cells activation), dopaminergic neuronal death (decreased TH^+ cell) in the SN, and motor dysfunctions (Fig. S1D). Collectively, the 16S rRNA results suggest that FLZ treatment attenuates the microbiota dysbiosis caused by rotenone.

3.7. *FLZ treatment suppresses intestinal inflammation and neuroinflammation by inhibiting TLR4/MyD88/NF-κB signaling pathway*

Capable of recognizing the bacterial product LPS, TLR4 has exerted its importance in the inflammation regulated by microbiota−gut−brain axis[45]. In addition, the pro-inflammatory cytokines which elevated in the rotenone-challenged mice are all the downstream products of TLR4/NF-κB signaling pathway[46,47]. Considering the changes in LPS and pro-inflammatory molecules that we demonstrated before, we hypothesized that the intestinal inflammation and neuroinflammation might be mediated through TLR4 signaling pathway. To verify our hypothesis, the expression of TLR4 pathway related proteins in both colon and SN samples was tested by Western blot, ELISA, immunofluorescence staining as well as qPCR. In the SN samples, Western blot results showed significantly increased protein expression of TLR4 ($P < 0.001$), MyD88 ($P < 0.01$), p-IκB-α ($P < 0.001$), NF-κB ($P < 0.001$) and reduced level of IκB-α protein expression ($P < 0.01$) in the Rotenone group compared to the Control group (Fig. 7A−F). On the contrary, FLZ treatment remarkably reversed these effects by decreasing the protein expression of TLR4 ($P < 0.001$), MyD88 ($P < 0.05$), p-IκB-α ($P < 0.001$), NF-κB ($P < 0.001$) and increasing the IκB-α expression ($P < 0.05$) (Fig. 7A−F). In addition, immunofluorescence staining further illustrated higher numbers of $TLR4^+$ cells in the Rotenone group than the Control group in the SN ($P < 0.001$) (Fig. 7O and P). In contrast, FLZ treatment reduced the numbers of $TLR4^+$ cells (Rotenone group, 24 cells/field; FLZ group, 12 cells/field; $P < 0.001$) (Fig. 7O and P). Consistent with Western blot and immunofluorescence results, qPCR results show that the mRNA expression of *Tlr4* increased in the SN ($P < 0.01$) of the Rotenone group mice, while FLZ administration suppressed the increased expression ($P < 0.05$) (Fig. 7S). As a result of activated TLR4 pathway, ELISA results illustrate the elevated level of TNF-α expression in the Rotenone group ($P < 0.001$) (Fig. 7G). However, TNF-α generation was markedly suppressed by FLZ treatment (Rotenone group, 0.75 pg/L; FLZ group, 0.56 pg/L; $P < 0.001$) (Fig. 7G). Besides, qPCR analysis further confirmed that mRNA expression of *Tnf* increased in the Rotenone group ($P < 0.01$) and FLZ treatment significantly suppressed its expression in the SN ($P < 0.01$) (Fig. 7T).

We also detected the TLR4 pathway related proteins in colon samples, which showed the same as the SN tissues. Compared to the Control group, the Rotenone group showed significantly elevated protein expression including TLR4 ($P < 0.05$), MyD88 ($P < 0.001$), p-IκB-α ($P < 0.001$) and NF-κB ($P < 0.01$) and decreased IκB-α protein expression ($P < 0.001$) (Fig. 7H−M). However, FLZ administration also showed significant inhibition of this pathway in the colon by decreasing the expression of proteins including TLR4 ($P < 0.001$), MyD88 ($P < 0.001$), p-IκB-α ($P < 0.001$), NF-κB ($P < 0.01$) and increasing IκB-α expression ($P < 0.01$) (Fig. 7H−M). Moreover, more $TLR4^+$ cells in the colon tissues of the Rotenone group than the Control group were detected by immunofluorescence staining ($P < 0.001$), which was suppressed by FLZ administration (Rotenone group, 12 cells/field; FLZ group, 1 cell/field; $P < 0.001$) (Fig. 7Q and R). Consistently, qPCR results showed that the mRNA expression of *Tlr4* elevated in the colon tissues of the Rotenone group mice ($P < 0.001$), while FLZ treatment inhibited the increased expression ($P < 0.001$) (Fig. 7S). In addition, ELISA analysis of colon samples illustrated higher TNF-α ($P < 0.001$) expression in the Rotenone group than the Control group (Fig. 7N). On the contrary, TNF-α expression was significantly inhibited by FLZ treatment (Rotenone group, 0.79 pg/L; FLZ group, 0.40 pg/L; $P < 0.001$) (Fig. 7N). Consistent with the ELISA results, qPCR analysis revealed that mRNA expression of *Tnf* elevated in the Rotenone group ($P < 0.01$) whereas FLZ treatment significantly suppressed its expression in the colon ($P < 0.05$) (Fig. 7T).

Taken together, all these results prove that TLR4/MyD88/NF-κB signaling pathway may contribute to the protective effects of FLZ treatment on the intestinal inflammation and neuroinflammation induced by rotenone.

4. Discussion

In our current study, we illustrated for the first time that FLZ treatment can remarkably attenuate the GI dysfunctions and motor symptoms in mice induced by rotenone. Further experiments proved that FLZ treatment can reduce the intestinal inflammation and barrier disruption, thereby suppressing the systemic inflammation to ameliorate the BBB impairment and neuroinflammation

The mRNA expression of *Tnf* in SN and colon. In (B)−(F) and (I)−(M), $n = 4$ for each group. In (G) and (N), $n = 8$ for each group. In (P) and (R), $n = 5$ for each group. In (S)−(T), $n = 3$ for each group. Data are presented as mean ± SD. $^{\#}P < 0.05$, $^{\#\#}P < 0.01$, $^{\#\#\#}P < 0.001$ *versus* the Control group; $^{*}P < 0.05$, $^{**}P < 0.01$, $^{***}P < 0.001$ *versus* the Rotenone group.

in rotenone-challenged mice. These protective effects of FLZ treatment on PD may stem from its beneficial influence on the composition of gut microbiota, which suppresses the TLR4/MyD88/NF-κB signaling pathway. Our results also suggested that microbiota−gut−brain axis plays an important role in the development of PD. The microbiota-related mechanisms of FLZ treatment for PD and the pathway of microbiota−gut−brain axis in PD development are illustrated in Fig. 8.

FLZ, a novel synthetic compound, was derived after chemical structure modification of squamosamide isolated from the traditional Chinese herb *Annona glabra*[48]. Our previous researches have proved the potent neuroprotective effects of FLZ in various PD models, including 1-methyl-4-phenyl-1,2,3,6-tetrahydropyridine (MPTP)-challenged PD model[17], 6-hydroxydopamine (6-OHDA)-induced *in vivo* and *in vitro* models[49], and mutant α-Syn (A53T) transgenic mouse model[24]. Moreover, FLZ treatment for PD has been approved by CFDA and is undergoing the phase I clinical trial. Further investigation demonstrated that the beneficial effects of FLZ on PD might result from its anti-inflammatory activity or its reduction on α-Syn aggregation[30,50]. We also found that the gut microbiota can regulate the absorption of FLZ, which indicated that the protective effects of FLZ treatment on PD is associated with gut microbiota.

To evaluate the protective effects of FLZ on PD and explore its association with gut microbiota composition alterations, chronic oral administration of rotenone was applied to mimic the development of both GI and motor symptoms in PD. Rotenone, known as insecticides, has been used to trigger PD animal models by targeting at mitochondrial complex I in several studies[51]. Inden et al.[27] reported that chronic treatment of rotenone replicated selective, dose-dependent dopaminergic neurodegeneration and cytoplasmic α-Syn accumulation in the SN of PD mouse model, leading to motor deficits. In addition, a recent report showed that the administration of rotenone for four weeks (30 mg/kg/day) could partially reproduce GI pathologies including declined fecal pellet output, and cause a decrease in TH-positive neurons[29]. Besides, another study conducted liquid chromatographic measurements as well as mitochondrial complex I activity analysis on the blood and brain samples of chronic rotenone-induced mice, which confirmed that no systemic distribution of rotenone existed in the brain[25]. This research proved that oral administration of rotenone only has local effects in the gut rather than any distant influence on the brain. In our current study, rotenone-intoxicated mice revealed an earlier presentation of GI dysfunctions at Week 3, including decreased intestinal transit, colon length and colon motility. Then, the development of motor deficits started from Week 4, which is consistent with a time-dependent longitudinal research on rotenone model[18]. In that study, α-Syn pathology in the colon was also observed prior to the degeneration of TH-positive neurons and the aggregation of α-Syn in the midbrain[18]. All these results together suggest that PD may derive from etiological factors in the gut, especially microbiota dysbiosis. Besides, our present study showed that 2-week FLZ treatment not only restored the GI functions but also alleviated the motor deficits, which confirmed its therapeutic effects on PD. Intriguingly, FLZ administration ameliorated GI dysfunctions 1 week earlier than motor symptoms, suggesting that the gut−brain axis regulated by microbes contributes to the protective effects of FLZ treatment on PD models.

It has been increasingly evident that altered microbiota composition is critical in the initiation of PD. Consistent with other studies of rotenone-induced PD models[18,52], we also found altered microbiota community structure in our mouse model as early as the fourth week. Moreover, FLZ treatment could modulate the destructed microbial community. At first, the differences of microbial distribution, abundance, and diversity among three groups were overviewed using alpha and beta diversity analysis. We found a decrease of alpha indices (Shannon and Simpson) comparing the Rotenone group to the Control group, which is also observed in other PD animal models[18,53]. Similarly, our beta diversity results demonstrated that the Rotenone group was remarkably separated from the Control group, which is consistent with other microbiota analyses of PD patients or animal models[12,18,54]. Meanwhile, diversity analysis showed that FLZ treatment could reverse the changes in alpha and beta diversity caused by rotenone administration. Taken together, these data suggested that FLZ treatment exerts protective effects on microbiota dysbiosis caused by rotenone from an overall perspective.

In addition, our 16S rRNA sequencing data revealed aberrant microbial composition at different taxa levels. At phylum level, the similar alterations in Verrucomicrobia and Bacteroidetes abundance caused by rotenone administration were consistent with other studies of PD patients or animal models[55−58]. On the contrary, we found that FLZ treatment could reverse these changes. In addition, one of the most important alterations of bacteria in our study was the significantly increased genus *Akkermansia* as well as its family Verrucomicrobiaceae and phylum Verrucomicrobia in the rotenone-induced mice. Consistently in another animal study, Dodiya et al.[56] discovered that the abundances of *Akkermansia* were also elevated in the rotenone-induced PD mouse model. More importantly, the increased level of *Akkermansia* was found to be present in fecal samples of PD patients[54,55,59,60]. Further mechanistic experiments on this bacterial genus suggested that *Akkermansia*, a Gram-negative bacterium, is able to degrade intestinal mucus barrier and make gut susceptible to pathogens, thus leading to local inflammation[16,61]. Besides, the abundance of *Akkermansia* is negatively associated with the expression of NLRP6, an innate immune receptor which protects animals from intestinal injuries[61]. All these findings partially explain the association of increased *Akkermansia* abundances and PD. In contrast, we also found that FLZ administration reversed the elevated *Akkermansia* abundance in the rotenone-induced mouse model, further suggesting that the regulation of microbes contributed to the protective effects of FLZ on rotenone-challenged mice. Moreover, higher prevalence of Hp infection has been found in PD patients[10,62,63]. On the contrary, lower relative abundance of genus *Helicobacter* was shown in our study, which might be caused by differences between PD patients and animal models. Additionally, we found FLZ treatment could preserve the alterations of some other bacterial genera in the mice challenged by rotenone. The levels of *Alistipes*[11] and *Barnesiella*[64] abundances are also reported to be related to PD. Their associations with gut inflammation may contribute to the alterations in PD patients[65,66]. However, *Enterorhabdus* and *Olsenella* are firstly reported to be related to PD in our study. The specific mechanisms of these bacterial genera in the development of PD still need more investigation. Furthermore, different KEGG pathways were then predicted based on these altered bacterial genera by functional analysis. Consistent with other fecal microbiota analyses of PD animal models or patients[18,54,59], putative pro-inflammatory pathways were also enriched in the rotenone-induced mice (*e.g.*, lipopolysaccharide biosynthesis, secretion system, xenobiotics biodegradation and metabolism, signaling molecules and interaction). The influences of gut microbiome on xenobiotics

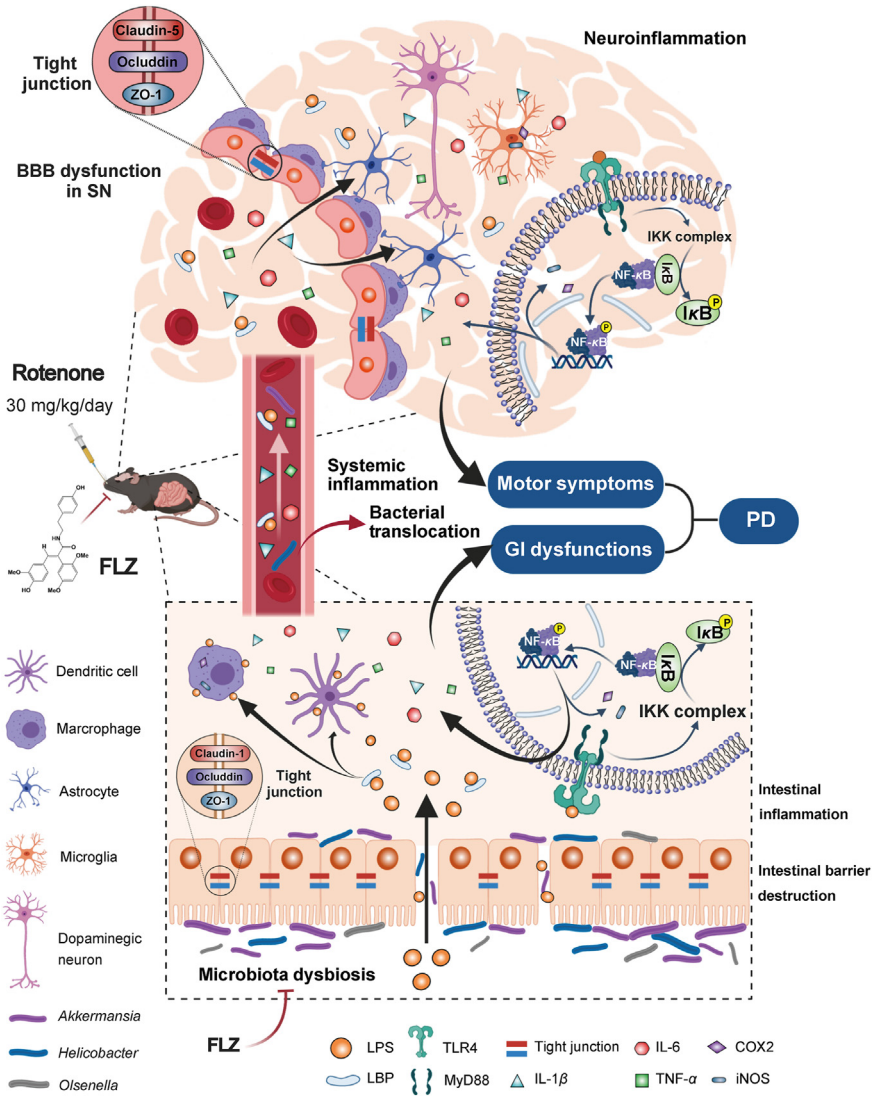

Figure 8 Schematic illustration of the microbiota-related mechanisms of FLZ treatment for PD and the pathway of microbiota−gut−brain axis in PD development. FLZ treatment can attenuate the PD-related disturbed microbial community (*e.g.*, *Akkermansia*, *Helicobacter*, and *Olsenella*) induced by rotenone to inhibit the release of LPS endotoxin and the generation of pro-inflammatory molecules including IL-1β, IL-6, TNF-α, COX2, and iNOS in the gut. The suppressed intestinal inflammation can further preserve the gut barrier destruction by protecting tight junction. Subsequently, lower levels of microbes, LPS, and pro-inflammatory cytokines (IL-1β, IL-6, and TNF-α) are released into the circulation, which suppresses the bacterial translocation and the systemic inflammation. Then, the blood−brain barrier structure is restored and lower levels of LPS and pro-inflammatory cytokines will cross the BBB to get into the SN, which inhibits the activation of microglia and astrocytes. The reduced neuroinflammation protects dopaminergic neurons from death. Further mechanistic study suggests that the protective effects of FLZ administration is mediated through suppressing the activation of TLR4/MyD88/NF-κB signaling pathway both in the gut and brain. Finally, FLZ administration attenuates GI dysfunctions and motor deficits in the rotenone-induced PD mouse model. This illustration summarizes how FLZ treatment ameliorates rotenone-induced PD mouse model by suppressing TLR4 pathway through microbiota−gut−brain axis. It also demonstrates that microbiota−gut−brain axis plays a critical role in PD pathogenesis.

metabolism have been reported recently[67]. The enrichment of LPS Biosynthesis pathway correlates with increased LPS levels in the feces and colon of the Rotenone group, indicating that microbiota dysbiosis in the rotenone-induced mice can enhance LPS generation and lead to the increased level of intestinal inflammation, while FLZ administration can reverse the process. In addition, our correlation analysis proves that these alterations in the microbiota community are strongly associated with following neuroinflammation and dopaminergic neuronal death. Collectively, FLZ treatment can restore several microbial taxa altered by rotenone at different levels to inhibit intestinal inflammation, further supporting that gut microbiota dysbiosis is important in the pathogenesis of PD.

Subsequently, several mechanistic experiments were conducted to explain how rotenone induced PD symptoms and FLZ treatment alleviated these symptoms through microbiota−gut−brain axis. Under normal circumstances, tight intestinal barrier and mucus restrict the microbiota to the surface of gut and our innate immune system protects the intestine from inflammatory reaction[20]. However, it is reported that chronic administration of rotenone

might induce sustained gut inflammation, resulting in harmful changes in gut microbiota community[9,18], which was also observed in our study. These deleterious effects would increase the intestinal permeability by regulating expression of tight junction proteins[19,21]. In the current research, bacterial translocation study found colony growth in germ-free organs of rotenone-intoxicated mice, further suggesting that intestinal damage caused by rotenone led to the leakage of microbes. Moreover, the FTIC-dextran assay, a widely used *in vivo* measurement for intestinal permeability, was applied. High concentration of 4 kDa FITC-dextran detected in the serum represents increased gut permeability. In our research, the *in vivo* FITC assay confirmed that FLZ treatment could reduce the permeability increased by rotenone. Finally, the TEM analysis of colon samples directly revealed that the destruction of tight junction in intestinal barriers was preserved by FLZ treatment. Further Western blot and qPCR analysis suggested that the barrier structure impairment might be caused by the suppression of tight junction proteins, including ZO-1, occludin, and claudin-1. In contrast, FLZ administration restored the barrier function *via* upregulating the expression of these tight junction proteins. In addition, the altered LPS levels in the colon and serum detected by ELISA analysis indicated that FLZ administration can attenuate the gut leakage induced by rotenone. Once LPS is translocated into intestinal tissues through impaired gut barrier, TLR4 on the surfaces of immune cells resident in the gut will recognize LPS. Then, MyD88-dependent signaling pathway is activated in the colon to generate more cytokines including IL-1β, IL-6, and TNF-α[68–70] as well as to increase the expression of pro-inflammatory molecules like iNOS[71] and COX2[47]. These cytokines and enzymes elevated by rotenone further leads to local inflammation in the gut. Multiple experiments, including western blot, immunofluorescence staining, ELISA, and qPCR, collectively proved that the activation of TLR4/MyD88/NF-κB pathway in the gut contributed to the elevated intestinal inflammation status in rotenone-intoxicated mice. On the contrary, FLZ treatment suppressed TLR4/MyD88/NF-κB pathway and decreased inflammatory proteins. To conclude, rotenone can increase the intestinal permeability and inflammation *via* TLR4 pathway while FLZ treatment can reverse these effects to restore the GI functions.

Intact BBB is important to protect the CNS from potentially harmful molecules whereas BBB dysfunction plays a great role in the pathogenesis of PD[43]. As a result of increased intestinal inflammation caused by rotenone, the elevated pathogen LPS, pro-inflammatory cytokines, and activated immune cells in the blood could induce systemic inflammation to impair the BBB and then directly interfere with the CNS to induce neuroinflammation[72,73]. In the current research, we detected increased LPS and LBP concentrations and elevated levels of pro-inflammatory cytokines in the serum of rotenone-induced mice, indicating that the activated systemic inflammation was induced by rotenone. On the contrary, the reduced levels in the FLZ group suggested that FLZ treatment can suppress the systemic inflammation, thereby restoring the disrupted BBB integrity in the rotenone-induced mice as illustrated in our TEM results. In addition, Western blot and immunofluorescence staining together revealed that FLZ administration preserved the inhibition of tight junction protein expression in the SN of the rotenone-induced mice. With the assistance of inflammatory cytokines, the ligand LPS as well as pro-inflammatory cytokines in the blood easily got access to the brain across the impaired BBB, which was proved by the elevated LPS levels in the SN. Then, the TLR4/MyD88/NF-κB pathway was stimulated in the SN, which locally increased the expression of inflammatory cytokines (IL-1β, IL-6, and TNF-α) and pro-inflammatory enzymes (COX2 and iNOS). As important local immune cells in the CNS, activated microglia and astrocytes contribute to further neuroinflammation and dopaminergic neurodegeneration[41,42,74]. Our experiments found that the excessive activation of inflammatory astrocytes and microglia correlated with dopaminergic neuron (TH-positive neuron) death in the SN region, which resulted in motor deficits of the rotenone-challenged PD mice. In addition, more CD3-positive T cells were also present in the SN region. Conversely, FLZ treatment preserved the BBB function and integrity through inhibiting systemic inflammation, thereby showing protective effects on neuroinflammation and neurodegeneration *via* suppressing the activation of microglia and astrocytes. In general, FLZ treatment exerts neuroprotective effects on the rotenone mouse model by restoring the BBB structure and function as well as inhibiting the pro-inflammatory activation of resident immune cells through suppressing TLR4/MyD88/NF-κB pathway.

The critical role of TLR4 pathway in the microbiota−gut−brain axis has also been reported in other researches. In a recent study, the knockout of TLR4 attenuated the intestinal inflammation, neuroinflammation and neurodegeneration in the rotenone-challenged mice, suggesting the critical role of TLR4 pathway in PD pathogenesis[46]. In addition, Sun et al.[75] reported that fecal microbiota transplantation reduced microbiota dysbiosis, thereby suppressing the intestinal inflammation and neuroinflammation *via* inhibiting TLR4/TBK1/NF-κB signaling pathway, and ultimately exerted neuroprotective effects on the MPTP mouse model. In the current research, we have further confirmed the important role of TLR4 pathway activation in the microbiota−gut−brain axis.

In our research, the microbiota dysbiosis in the rotenone-induced mouse model elevated the intestinal inflammation and gut barrier permeability. Then, the increased LPS and inflammatory cytokines would be leaked into the circulation, thereby causing systematic inflammation. Consequently, the BBB was disrupted and neuroinflammation was induced in the SN, which led to the development of the rotenone-challenged mice. However, FLZ administration could arrest the whole process and alleviate PD symptoms induced by rotenone. The protective effects of FLZ treatment on PD and its microbiota-related mechanisms suggest that microbiota−gut−brain axis plays an important role in PD pathogenesis, which is a potential target for PD treatment.

5. Conclusions

Our findings report for the first time that the novel compound FLZ can attenuate the GI dysfunctions in addition to motor deficits in the rotenone-intoxicated PD mouse model, suggesting the vital role of gut microbiota in these protective effects. Furthermore, FLZ treatment modulates the microbiota−gut−brain axis through inhibiting the activation of TLR4/MyD88/NF-κB signaling pathway both in the gut and brain. Current research provides evidence that FLZ treatment attenuates microbiota dysbiosis to protect the PD mouse model through inhibiting TLR4 pathway, which contributes to one of the underlying mechanisms beneath its protective effects. We also prove the importance of microbiota−gut−brain axis in PD pathogenesis, suggesting its potential role as a novel therapeutic target for PD treatment.

Acknowledgments

This work was supported by grants from National Sciences Foundation of China (81773718, 81630097, and 81773589), The National Key Research and Development Program of China (Grant No. SQ2018YFA090025-04), CAMS Innovation Fund for Medical Sciences (No. 2016-I2M-3−011, China), The Drug Innovation Major Project (2018ZX09711001-003-020, 2018ZX09711001-003-005, and 2018ZX09711001-008-005, China), CAMS The Fundamental Research Funds for the Central Universities (2018RC350002, China), CAMS & PUMC Innovation Fund for Graduate (No. 2019-1007-23, China).

Author contributions

We declare that all authors made fundamental contributions to the manuscript. Zhe Zhao and Dan Zhang designed the study. Zhe Zhao, Fangyuan Li, Jingwen Ning, and Ran Peng carried out experiments. Junmei Shang, Meiyu Shang, and Hui Liu analyzed the data. Zhe Zhao prepared the manuscript. Dan Zhang and Xiuqi Bao advised the experiment. All authors revised the manuscript and approved the final version.

Conflicts of interest

All authors declare no competing interests.

Appendix A. Supporting information

Supporting data to this article can be found online at https://doi.org/10.1016/j.apsb.2021.03.020.

References

1. Tysnes OB, Storstein A. Epidemiology of Parkinson's disease. *J Neural Transm* 2017;**124**:901−5.
2. Jankovic J. Parkinson's disease: clinical features and diagnosis. *J Neurol Neurosurg Psychiatry* 2008;**79**:368−76.
3. Beach TG, Adler CH, Sue LI, Vedders L, Lue L, White III CL, et al. Multi-organ distribution of phosphorylated alpha-synuclein histopathology in subjects with Lewy body disorders. *Acta Neuropathol* 2010;**119**:689−702.
4. Caputi V, Giron MC. Microbiome−gut−brain axis and Toll-like receptors in Parkinson's disease. *Int J Mol Sci* 2018;**19**:1689.
5. Kalia LV, Lang AE. Parkinson's disease. *Lancet* 2015;**386**:896−912.
6. Fasano A, Visanji NP, Liu LW, Lang AE, Pfeiffer RF. Gastrointestinal dysfunction in Parkinson's disease. *Lancet Neurol* 2015;**14**:625−39.
7. Kim JS, Sung HY. Gastrointestinal autonomic dysfunction in patients with Parkinson's disease. *J Mod Dynam* 2015;**8**:76−82.
8. Klingelhoefer L, Reichmann H. Pathogenesis of Parkinson disease—the gut−brain axis and environmental factors. *Nat Rev Neurol* 2015;**11**:625−36.
9. Mulak A, Bonaz B. Brain−gut−microbiota axis in Parkinson's disease. *World J Gastroenterol* 2015;**21**:10609−20.
10. Charlett A, Dobbs RJ, Dobbs SM, Weller C, Brady P, Peterson DW. Parkinsonism: siblings share *Helicobacter pylori* seropositivity and facets of syndrome. *Acta Neurol Scand* 1999;**99**:26−35.
11. Bedarf JR, Hildebrand F, Coelho LP, Sunagawa S, Bahram M, Goeser F, et al. Functional implications of microbial and viral gut metagenome changes in early stage L-DOPA-naïve Parkinson's disease patients. *Genome Med* 2017;**9**:39.
12. Scheperjans F, Aho V, Pereira PA, Koskinen K, Paulin L, Pekkonen E, et al. Gut microbiota are related to Parkinson's disease and clinical phenotype. *Mov Disord* 2015;**30**:350−8.
13. Sun MF, Shen YQ. Dysbiosis of gut microbiota and microbial metabolites in Parkinson's disease. *Ageing Res Rev* 2018;**45**:53−61.
14. de Theije CG, Wopereis H, Ramadan M, van Eijndthoven T, Lambert J, Knol J, et al. Altered gut microbiota and activity in a murine model of autism spectrum disorders. *Brain Behav Immun* 2014;**37**:197−206.
15. Sampson TR, Mazmanian SK. Control of brain development, function, and behavior by the microbiome. *Cell Host Microbe* 2015;**17**:565−76.
16. Desai MS, Seekatz AM, Koropatkin NM, Kamada N, Hickey CA, Wolter M, et al. A dietary fiber-deprived gut microbiota degrades the colonic mucus barrier and enhances pathogen susceptibility. *Cell* 2016;**167**:1339−1353.e21.
17. Bao XQ, Kong XC, Qian C, Zhang D. FLZ protects dopaminergic neuron through activating protein kinase B/mammalian target of rapamycin pathway and inhibiting RTP801 expression in Parkinson's disease models. *Neuroscience* 2012;**202**:396−404.
18. Yang X, Qian Y, Xu S, Song Y, Xiao Q. Longitudinal analysis of fecal microbiome and pathologic processes in a rotenone induced mice model of Parkinson's disease. *Front Aging Neurosci* 2017;**9**:441.
19. Capaldo CT, Nusrat A. Cytokine regulation of tight junctions. *Biochim Biophys Acta* 2009;**1788**:864−71.
20. Al-Asmakh M, Hedin L. Microbiota and the control of blood−tissue barriers. *Tissue Barriers* 2015;**3**:e1039691.
21. Houser MC, Tansey MG. The gut−brain axis: is intestinal inflammation a silent driver of Parkinson's disease pathogenesis?. *NPJ Parkinsons Dis* 2017;**3**:3.
22. Pavlov VA, Tracey KJ. Neural circuitry and immunity. *Immunol Res* 2015;**63**:38−57.
23. Wong D, Dorovini-Zis K, Vincent SR. Cytokines, nitric oxide, and cGMP modulate the permeability of an *in vitro* model of the human blood−brain barrier. *Exp Neurol* 2004;**190**:446−55.
24. Bao XQ, Wang XL, Zhang D. FLZ attenuates alpha-synuclein-induced neurotoxicity by activating heat shock protein 70. *Mol Neurobiol* 2017;**54**:349−61.
25. Pan-Montojo F, Anichtchik O, Dening Y, Knels L, Pursche S, Jung R, et al. Progression of Parkinson's disease pathology is reproduced by intragastric administration of rotenone in mice. *PLoS One* 2010;**5**:e8762.
26. Inden M, Kitamura Y, Abe M, Tamaki A, Takata K, Taniguchi T. Parkinsonian rotenone mouse model: reevaluation of long-term administration of rotenone in C57BL/6 mice. *Biol Pharm Bull* 2011;**34**:92−6.
27. Inden M, Kitamura Y, Takeuchi H, Yanagida T, Takata K, Kobayashi Y, et al. Neurodegeneration of mouse nigrostriatal dopaminergic system induced by repeated oral administration of rotenone is prevented by 4-phenylbutyrate, a chemical chaperone. *J Neurochem* 2007;**101**:1491−504.
28. Johnson ME, Bobrovskaya L. An update on the rotenone models of Parkinson's disease: their ability to reproduce the features of clinical disease and model gene-environment interactions. *Neurotoxicology* 2015;**46**:101−16.
29. Tasselli M, Chaumette T, Paillusson S, Monnet Y, Lafoux A, Huchet-Cadiou C, et al. Effects of oral administration of rotenone on gastrointestinal functions in mice. *Neuro Gastroenterol Motil* 2013;**25**:e183−93.
30. Bao XQ, Wu LY, Wang XL, Sun H, Zhang D. Squamosamide derivative FLZ protected tyrosine hydroxylase function in a chronic MPTP/probenecid mouse model of Parkinson's disease. *Naunyn-Schmiedeberg's Arch Pharmacol* 2015;**388**:549−56.
31. Perez-Pardo P, de Jong EM, Broersen LM, van Wijk N, Attali A, Garssen J, et al. Promising effects of neurorestorative diets on motor, cognitive, and gastrointestinal dysfunction after symptom development in a mouse model of Parkinson's disease. *Front Aging Neurosci* 2017;**9**:57.
32. Zhao Z, Bao XQ, Zhang Z, Li F, Liu H, Zhang D. Novel phloroglucinol derivative Compound 21 protects experimental autoimmune

encephalomyelitis rats *via* inhibiting Th1/Th17 cell infiltration. *Brain Behav Immun* 2020;**87**:751−64.
33. Masella AP, Bartram AK, Truszkowski JM, Brown DG, Neufeld JD. PANDAseq: paired-end assembler for illumina sequences. *BMC Bioinf* 2012;**13**:31.
34. Edgar RC. UPARSE: highly accurate OTU sequences from microbial amplicon reads. *Nat Methods* 2013;**10**:996−8.
35. Wang Q, Garrity GM, Tiedje JM, Cole JR. Naive Bayesian classifier for rapid assignment of rRNA sequences into the new bacterial taxonomy. *Appl Environ Microbiol* 2007;**73**:5261−7.
36. Cole JR, Wang Q, Fish JA, Chai B, McGarrell DM, Sun Y, et al. Ribosomal Database Project: data and tools for high throughput rRNA analysis. *Nucleic Acids Res* 2014;**42**:D633−42.
37. Kemp PF, Aller JY. Bacterial diversity in aquatic and other environments: what 16S rDNA libraries can tell us. *FEMS Microbiol Ecol* 2004;**47**:161−77.
38. Segata N, Izard J, Waldron L, Gevers D, Miropolsky L, Garrett WS, et al. Metagenomic biomarker discovery and explanation. *Genome Biol* 2011;**12**:R60.
39. Langille MG, Zaneveld J, Caporaso JG, McDonald D, Knights D, Reyes JA, et al. Predictive functional profiling of microbial communities using 16S rRNA marker gene sequences. *Nat Biotechnol* 2013;**31**:814−21.
40. Zhao Z, Bao XQ, Zhang Z, Liu H, Zhang D. Phloroglucinol derivative compound 21 attenuates cuprizone-induced multiple sclerosis mice through promoting remyelination and inhibiting neuroinflammation. *Sci China Life Sci* 2020;**63**:905−14.
41. Booth HDE, Hirst WD, Wade-Martins R. The role of astrocyte dysfunction in Parkinson's disease pathogenesis. *Trends Neurosci* 2017;**40**:358−70.
42. Depboylu C, Stricker S, Ghobril JP, Oertel WH, Priller J, Höglinger GU. Brain-resident microglia predominate over infiltrating myeloid cells in activation, phagocytosis and interaction with T-lymphocytes in the MPTP mouse model of Parkinson disease. *Exp Neurol* 2012;**238**:183−91.
43. Desai BS, Monahan AJ, Carvey PM, Hendey B. Blood−brain barrier pathology in Alzheimer's and Parkinson's disease: implications for drug therapy. *Cell Transplant* 2007;**16**:285−99.
44. Gerhardt S, Mohajeri MH. Changes of colonic bacterial composition in Parkinson's disease and other neurodegenerative diseases. *Nutrients* 2018;**10**:708.
45. Yang X, Yu D, Xue L, Li H, Du J. Probiotics modulate the microbiota−gut−brain axis and improve memory deficits in aged SAMP8 mice. *Acta Pharm Sin B* 2020;**10**:475−87.
46. Perez-Pardo P, Dodiya HB, Engen PA, Forsyth CB, Huschens AM, Shaikh M, et al. Role of TLR4 in the gut−brain axis in Parkinson's disease: a translational study from men to mice. *Gut* 2019;**68**:829−43.
47. Ibáñez F, Montesinos J, Ureña-Peralta JR, Guerri C, Pascual M. TLR4 participates in the transmission of ethanol-induced neuroinflammation *via* astrocyte-derived extracellular vesicles. *J Neuroinflammation* 2019;**16**:136.
48. Zhang D, Hu X, Wei SJ, Liu J, Gao H, Qian L, et al. Squamosamide derivative FLZ protects dopaminergic neurons against inflammation-mediated neurodegeneration through the inhibition of NADPH oxidase activity. *J Neuroinflammation* 2008;**5**:21.
49. Bao XQ, Kong XC, Kong LB, Wu LY, Sun H, Zhang D. Squamosamide derivative FLZ protected dopaminergic neuron by activating Akt signaling pathway in 6-OHDA-induced *in vivo* and *in vitro* Parkinson's disease models. *Brain Res* 2014;**1547**:49−57.
50. Li DC, Bao XQ, Wang XL, Sun H, Zhang D. A novel synthetic derivative of squamosamide FLZ inhibits the high mobility group box 1 protein-mediated neuroinflammatory responses in murine BV2 microglial cells. *Naunyn-Schmiedeberg's Arch Pharmacol* 2017;**390**:643−50.
51. Chia SJ, Tan EK, Chao YX. Historical perspective: models of Parkinson's disease. *Int J Mol Sci* 2020;**21**:2464.
52. Johnson ME, Stringer A, Bobrovskaya L. Rotenone induces gastrointestinal pathology and microbiota alterations in a rat model of Parkinson's disease. *Neurotoxicology* 2018;**65**:174−85.
53. Lai F, Jiang R, Xie W, Liu X, Tang Y, Xiao H, et al. Intestinal pathology and gut microbiota alterations in a methyl-4-phenyl-1,2,3,6-tetrahydropyridine (MPTP) mouse model of Parkinson's disease. *Neurochem Res* 2018;**43**:1986−99.
54. Keshavarzian A, Green SJ, Engen PA, Voigt RM, Naqib A, Forsyth CB, et al. Colonic bacterial composition in Parkinson's disease. *Mov Disord* 2015;**30**:1351−60.
55. Heintz-Buschart A, Pandey U, Wicke T, Sixel-Döring F, Janzen A, Sittig-Wiegand E, et al. The nasal and gut microbiome in Parkinson's disease and idiopathic rapid eye movement sleep behavior disorder. *Mov Disord* 2018;**33**:88−98.
56. Dodiya HB, Forsyth CB, Voigt RM, Engen PA, Patel J, Shaikh M, et al. Chronic stress-induced gut dysfunction exacerbates Parkinson's disease phenotype and pathology in a rotenone-induced mouse model of Parkinson's disease. *Neurobiol Dis* 2020;**135**:104352.
57. Unger MM, Spiegel J, Dillmann KU, Grundmann D, Philippeit H, Bürmann J, et al. Short chain fatty acids and gut microbiota differ between patients with Parkinson's disease and age-matched controls. *Park Relat Disord* 2016;**32**:66−72.
58. Li W, Wu X, Hu X, Wang T, Liang S, Duan Y, et al. Structural changes of gut microbiota in Parkinson's disease and its correlation with clinical features. *Sci China Life Sci* 2017;**60**:1223−33.
59. Hill-Burns EM, Debelius JW, Morton JT, Wissemann WT, Lewis MR, Wallen ZD, et al. Parkinson's disease and Parkinson's disease medications have distinct signatures of the gut microbiome. *Mov Disord* 2017;**32**:739−49.
60. Li C, Cui L, Yang Y, Miao J, Zhao X, Zhang J, et al. Gut microbiota differs between Parkinson's disease patients and healthy controls in Northeast China. *Front Mol Neurosci* 2019;**12**:171.
61. Seregin SS, Golovchenko N, Schaf B, Chen J, Pudlo NA, Mitchell J, et al. NLRP6 protects IL10$^{-/-}$ mice from colitis by limiting colonization of *Akkermansia muciniphila*. *Cell Rep* 2017;**19**:733−45.
62. Huang HK, Wang JH, Lei WY, Chen CL, Chang CY, Liou LS. *Helicobacter pylori* infection is associated with an increased risk of Parkinson's disease: a population-based retrospective cohort study. *Park Relat Disord* 2018;**47**:26−31.
63. Lee WY, Yoon WT, Shin HY, Jeon SH, Rhee PL. *Helicobacter pylori* infection and motor fluctuations in patients with Parkinson's disease. *Mov Disord* 2008;**23**:1696−700.
64. Hopfner F, Künstner A, Müller SH, Künzel S, Zeuner KE, Margraf NG, et al. Gut microbiota in Parkinson disease in a northern German cohort. *Brain Res* 2017;**1667**:41−5.
65. Saulnier DM, Riehle K, Mistretta TA, Diaz MA, Mandal D, Raza S, et al. Gastrointestinal microbiome signatures of pediatric patients with irritable bowel syndrome. *Gastroenterology* 2011;**141**:1782−91.
66. Weiss GA, Chassard C, Hennet T. Selective proliferation of intestinal *Barnesiella* under fucosyllactose supplementation in mice. *Br J Nutr* 2014;**111**:1602−10.
67. Collins SL, Patterson AD. The gut microbiome: an orchestrator of xenobiotic metabolism. *Acta Pharm Sin B* 2020;**10**:19−32.
68. Kawasaki T, Kawai T. Toll-like receptor signaling pathways. *Front Immunol* 2014;**5**:461.
69. Płóciennikowska A, Hromada-Judycka A, Borzęcka K, Kwiatkowska K. Co-operation of TLR4 and raft proteins in LPS-induced pro-inflammatory signaling. *Cell Mol Life Sci* 2015;**72**:557−81.
70. Dantzer R, O'Connor JC, Freund GG, Johnson RW, Kelley KW. From inflammation to sickness and depression: when the immune system subjugates the brain. *Nat Rev Neurosci* 2008;**9**:46−56.

71. Lowenstein CJ, Padalko E. iNOS (NOS2) at a glance. *J Cell Sci* 2004; **117**:2865−7.
72. Biesmans S, Meert TF, Bouwknecht JA, Acton PD, Davoodi N, De Haes P, et al. Systemic immune activation leads to neuroinflammation and sickness behavior in mice. *Mediat Inflamm* 2013;**2013**:271359.
73. Erickson MA, Hansen K, Banks WA. Inflammation-induced dysfunction of the low-density lipoprotein receptor-related protein-1 at the blood−brain barrier: protection by the antioxidant *N*-acetylcysteine. *Brain Behav Immun* 2012;**26**:1085−94.
74. Dutta G, Barber DS, Zhang P, Doperalski NJ, Liu B. Involvement of dopaminergic neuronal cystatin C in neuronal injury-induced microglial activation and neurotoxicity. *J Neurochem* 2012;**122**: 752−63.
75. Sun MF, Zhu YL, Zhou ZL, Jia XB, Xu YD, Yang Q, et al. Neuroprotective effects of fecal microbiota transplantation on MPTP-induced Parkinson's disease mice: gut microbiota, glial reaction and TLR4/TNF-α signaling pathway. *Brain Behav Immun* 2018;**70**: 48−60.